G. Ghatak, A. De Domenico and M. Coupechou, "Small Cell Deployment Along Roads: Coverage Analysis and Slice-Aware RAT Selection," in *IEEE Transactions on Communications*.

doi: 10.1109/TCOMM.2019.2916794

Small Cell Deployment Along Roads: Coverage Analysis and Slice-Aware RAT Selection

Gourab Ghatak*, Antonio De Domenico†, and Marceau Coupechoux‡

*Indraprastha Institute of Information Technology Delhi (IIIT D), India; †CEA, LETI, MINATEC, Grenoble, France; ‡LTCI, Telecom ParisTech, Université Paris Saclay, France.

Email: gourab.ghatak@iiitd.ac.in; antonio.de-domenico@cea.fr, and marceau.coupechoux@telecom-paristech.fr

***Abstract*—We characterize a multi-tier wireless network consisting of multi radio access technology (RAT) small cells, operating in both sub-6GHz and millimeter wave (mm-wave) bands, overlaid on top of traditional macro cells. To realistically characterize the user equipment (UE) performance, we model the position of the small cells along roads. First, we provide tractable, yet realistic models to characterize the mm-wave interference and the effect of vehicular blockages on the mm-wave signals. Then, we introduce an association policy, where a UE selects the serving tier using the powers measured on the sub-6GHz band, and then, using the biased power of the mm-wave band, selects the RAT. Based on this, we derive the signal to interference plus noise ratio (SINR) coverage probabilities of pedestrian UEs. We investigate the effect of the RAT selection bias on the vehicular blockage, SINR coverage, and rate coverage experienced by the UEs. Leveraging the results of our analysis, we propose to use a varied range of RAT selection biases to support the diverse applications of the fifth generation (5G) mobile networks. Accordingly, we provide a slice-aware RAT selection strategy to support three types of services, characterized by different requirements in terms of reliability, coverage, and data rates.**

I. Introduction

Future wireless applications anticipate an explosion in the plethora of use-cases, which cannot be sustained by incremental improvements on the existing communication schemes [2]. To address this, exploiting millimeter wave (mm-wave) spectrum for broadband services is gaining popularity. Additionally, mm-wave communications employ directional antennas, which reduces co-channel interference, thereby improving the performance at the user equipment (UE) [3]. However, mm-wave transmissions suffer from detrimental path-losses and high sensitivity to blockages [4]. For example, a vehicle located between a base station (BS) and a pedestrian UE may block the signal and induce a temporary service outage. To mitigate the path-loss, beam-forming techniques should be adopted, which poses issues in terms of coverage and initial access [5]. One solution to this problem consists of enabling the UEs to simultaneously receive signals in the mm-wave and in the sub-6GHz band, and to use the sub-6GHz to support the initial access on the mm-wave band [6].

Thus, it is unrealistic to assume ubiquitous coverage with only mm-wave small cell base station (SBS)s, and it is envisioned that multiple radio access techniques (RATs) will co-exist in future [6]. The ad-hoc deployments of SBSs using multiple RATs will lead to a complex heterogeneous architecture. For example, in an urban scenario, the mm-wave SBSs can be deployed along the urban infrastructure, e.g., on top of lamp-posts [7]. Accordingly, it is important to characterize such a multi-tier multi-RAT network, and derive algorithms to optimize the UE and network performance, and fully exploit the potential gains from mm-wave SBS deployment. In this paper, we model a multi-tier network operating in sub-6GHz and mm-wave bands, where the SBSs are deployed along the roads. We characterize the UE performance in terms of signal to interference plus noise ratio (SINR) coverage probability, rate coverage probability, and vehicular blockages.

In the fourth generation (4G) networks, tier selection biasing is used mainly for load balancing. Offloading the UEs from the macro base station (MBS) to the SBSs is facilitated by a network-wide bias to expand the range of SBSs. On the contrary, we propose to use various RAT selection biases, each one associated to one of the services in the system and designed to carefully satisfy the service requirements. To sustain the diverse use cases of fifth generation (5G), a mobile operator will be able to define service-based logical partitions of its network over a common physical infrastructure. *Network slicing* facilitates the creation and management of such network instantiations (the network slices), each one composed by functions and parameters (e.g., the RAT bias in our work) tailored to address specific requirements [8]. In our work, we follow the specifications by 3GPP TS 23.501 [9], wherein a user initially facilitates connection to the network and sends a message through the signalling path, which consists of a Network Slice Selection Assistance Information (NSSAI). This is a set tuples containing information about slice type, slice differentiator etc. Following this, the access network selects an appropriate access function and forwards the NSSAI to it. Then the access function decides the set of allowed slice types for the user, using the information in NSSAI, the device capabilities, the user's profile, and the policy of the network operator. Indeed, until this point there is no reservation of physical resources. After the user, based on its service request, associates with one of the slices offered by the network, the bias value of the concerned slice is used for selection of the RAT in case the association is with an SBS.

A part of this paper was presented in IEEE Globecom 2017 [1]. Part of this work has been performed within the 5G-MoNArch project (Grant Agreement No. 761445), part of the Phase II of the 5th Generation Public Private Partnership (5G-PPP) program partially funded by the European Commission within the Horizon 2020 Framework Program. A major part of this work was completed when G. Ghatak was affiliated to CEA-LETI and Telecom ParisTech.

A. Related Work

In heterogeneous networks, the UE performance is analyzed using stochastic geometry by calculating the SINR coverage probability and rate coverage probability [10]. These metrics have been derived to investigate single-tier [11] and multi-tier mm-wave networks [12], as well as multi-RAT networks with mm-wave SBSs [13]. In literature, multi-tier networks are modeled using homogeneous two dimensional Poisson point process (PPP) [12], [13] or using repulsive processes [14]. These models, although tractable, are not able to capture the urban deployment of SBSs along the metropolitan infrastructure, e.g., along the roads and on lamp posts. For example, traditional models of such networks either consider only the proximity of the BS for UE association [13], or characterize UE association by modeling mm-wave link blockages using distance-based line-of-sight (LOS) ball models [12]. However, a BS located sufficiently close, but on a different street than that of a UE may not provide sufficient downlink power to the UE due to blockages by buildings, which is not straightforward to capture using single or multiple LOS ball models. In our work we address this issue by studying the performance of on-road deployment of mm-wave SBSs in a dense blocking environment.

In this regard, Gloaguen *et al.* [15] have modeled roads using either a Poisson-line tessellation (PLT), Poisson-Voronoi tessellation, or a Poisson-Delaunay tessellation. Specifically, using the PLT model, they have analyzed a two-tier wired network with respect to the mean shortest path length and the mean subscriber line length. The PLT was used by Morlot [16] to model the location of UEs and by Choi and Baccelli [17] to model vehicular BSs and UEs. In our previous work [1], we have characterized a multi-RAT network using SBS deployments based on a PLT and performed a first coverage analysis for pedestrian UEs.

Furthermore, the effect of the blockages due to vehicular traffic on the pedestrian UE performance is generally ignored. This inhibits a realistic study of the mm-wave cellular networks, since vehicular blockage is an integral part of a metropolitan scenario. Recently, Tassi *et al.* [18] have investigated a highway scenario with moving vehicles modeled as rectangles on the lanes. In our work, we model vehicles as cuboids, and analyze the effect of vehicular blockages on the pedestrian UE performance. Accordingly, we have revealed unique features of the network, especially related to how the UEs are distributed across various RATs to satisfy the associated slice requirements for varying degrees of link blockage due to the vehicles. Measurement campaigns affirm that in a street light based SBS deployment, the physical structures like buildings, vehicles etc. will be critical for performance evaluation [19]. Therefore, our model that takes into account blockages due to buildings and moving vehicles presents a very realistic characterization of such a network.

Finally, Foukas *et al.* [8] have provided a survey of the challenges in 5G network slicing. They have identified that the multiplexing of different RATs is *the* main challenge for resource virtualization. In this paper, we provide a first study in this direction, in the context of multi-RAT multi-tier networks, by proposing a RAT selection mechanism that associates a RAT bias to each of the network slices deployed by the network operator, each of them characterized by a specific set of QoS requirements.

B. Contributions and Organization

1) We use the Poisson line process (PLP) to model the roads of an urban scenario on which multi-RAT SBSs, operating in both sub-6GHz and mm-wave bands are deployed to serve pedestrian UEs. Although this scenario is widely envisioned for future networks architectures, the investigation of such multi-tier, multi-RAT network has not yet been performed in the literature to the best of our knowledge. Thus, our analysis provides more reliable results in terms of association probabilities and SINR coverage probabilities as compared to the traditional models.

2) We propose a mm-wave interference model for SBS deployment along roads. For that, we derive the worst-case probability of the interference perceived at a UE from the n-th neighboring SBS. Then, we show that the accurate characterization of the mm-wave interference in presence of vehicular blockages is analytically difficult. We thus introduce a tractable dominant-interferer based interference model. We show that our model is more accurate in characterizing the SINR coverage as compared to a noise-limited approach, which is adopted for simple design of resource allocation and interference management mechanisms in mm-wave networks, see e.g. [20].

3) We consider the effect of the vehicles that cause a temporary blockage in the LOS link between an outdoor UE and the SBSs. We exploit the properties of the Poisson line Cox process (PLCP) to characterize the average vehicular blockage probability of a pedestrian UE from its serving SBS. This enables the operators to properly dimension the network so as to cater to the needs of reliability constrained applications. Although vehicular blockages are considered in studying vehicular communications [18], our model is the first tractable approach to analyze the UE performance in a multi-tier multi-RAT networks.

4) We propose a two-step association policy where the UEs are connected to a tier based on the maximum received power in the sub-6GHz band. In case the UE associates to an SBS, it requests service from the RAT that provides the maximum biased instantaneous downlink received power. We compare this association scheme with an approach that uses an averaged power measured over a longer duration. We highlight that the first scheme suffers from an upper bound on the mm-wave selection probability, due to the vehicular blockages, and thus hampers aggressive mm-wave offloading. Using the derived results of the PLCP and the association probabilities with various tiers and RATs, we derive the SINR coverage probabilities for the UEs.

5) Our results show that for a given density of the SBSs and vehicles, the optimal RAT selection bias should vary for addressing different service requirements, e.g., service reliability, coverage, and data rate. Accordingly, we consider different classes of services, namely ultra-reliable low-latency communications (URLLC), massive machine-type communications

(mMTC), and enhanced mobile broadband (eMBB) [21], and provide to the operator an algorithm to tune the RAT selection bias, in order to support their requirements.

The rest of the paper is organized as follows. In Section II, we present some preliminary results on the PLCP. In Section III, we introduce our system model. In Section IV, we characterize the vehicular blockage and mm-wave interference. The association probabilities and the SINR coverage probabilities are derived in Section V and Section VI, respectively. In Section VII we present our slice-aware RAT selection strategy. Simulation results are provided in Section VIII. Finally, the paper concludes in Section IX.

II. Preliminary Results on PLCP

In this section, we present the construction and some salient properties of the PLCP. For that, we first describe the formation of a PLP, which will act as the domain of the PLCP.

A. PLCP Definition

A line process $\mathcal{P} \subset \mathbb{R}^2$ is a collection of random lines $\{L_1, L_2, \ldots\}$ in the Euclidean plane. Any line that belongs to $\mathcal{P}$ is uniquely characterized by the distance d between the origin O and its projection P on the line, and by the angle ψ between $\vec{OP}$ and the x-axis on the other hand. Let the domain of the pair of parameters (ψ, d) be the half cylinder $\mathcal{C} := [0, 2\pi) \times \mathbb{R}^+$. We will call $\mathcal{C}$ as the generating set of $\mathcal{P}$, and a point $x_i \in \mathcal{C}$, corresponding to a line $L_i \in \mathcal{P}$, the generating point of L_i. Accordingly, there is a bijective mapping $f : \mathcal{P} \to \mathcal{C}$ between any random point $x_i \in \mathcal{C}$ and a corresponding line $L_i \in \mathcal{P}$. We can now define a PLP.

Definition 1. *A line process $\mathcal{P} \triangleq \{L_i\}$ in $\mathbb{R}^2$ is a PLP, if and only if the set of corresponding generating points $\{x_i = f(L_i)\}$ is a PPP in $\mathcal{C}$.*

On every line $L_i \in \mathcal{P}$, we define a one-dimensional PPP (ϕ_i), with intensity λ_S. The collection of all such points on all the lines of $\mathcal{P}$ is a PLCP, denoted ϕ_S. Thus, the resulting point process is doubly stochastic, with the density concentrated along the lines. Naturally, $\phi_S = \cup_{i \in \mathcal{P}} \phi_i$.

Definition 2. *A PLCP based on a PLP $\mathcal{P}$, is a process driven by a measure λ_S given by: $\lambda_S(B) = N\ell_1(\mathcal{P} \cap B)$, for a Borel set B, where N is a positive constant and ℓ_1 is the total length of all the lines of $\mathcal{P}$ in B.*

Definition 3. *Two points x and x' are neighbors to each other, if and only if $\exists i$: $x, x' \in \phi_i$. Thus, from the perspective of one point x, all the neighbors on either side of it can be enumerated as n-th neighbors, where $n \in \mathbb{N}\backslash\{0\}$.*

B. Palm Perspective of the PLCP

Let us study the PLCP from the perspective of a point of the process itself, using Palm calculus[2]. Thanks to the Slivnyak's theorem [22] for a PPP (ϕ), conditioning on the event that a point of ϕ is located at the origin (o) (in other words $o \in \phi$), is equivalent to *add* a point at o to the PPP ϕ. Mathematically, $\mathbb{P}(\phi \in Y | o) = \mathbb{P}(\phi \cup \{o\} \in Y)$, where Y is any point process property. On similar lines, we state the following Lemma for a PLCP [16].

Lemma 1. *For a PLCP $\mathcal{P}$, we have $\mathbb{P}(\phi_S \in Y | o) = \mathbb{P}(\phi_S \cup \phi_0 \cup \{o\} \in Y)$, where ϕ_0 is a realization of ϕ_i which passes through the origin.*

In other words, Palm distribution i.e., conditioning on a point of ϕ_S to be at the origin, is equivalent to *add* (i) an independent Poisson process of intensity λ_S on a line through the origin with uniform independent angle and (ii) an atom at the origin to the PLCP. The implication of this result is observed in several results that we derive in this work. As an example, assume the SBSs are distributed as a PLCP. Then, if a UE is associated with an SBS located at x, then we have to condition the SBS process based on the fact that there exists a point of the SBS process located at x. This directly implies that the corresponding Palm process must include a line (road) containing SBSs passing through x.

C. Probability Generating Functionals of the PLCP

Here, we introduce the notion of the probability generating functional (PGF) of the point processes. The PGF of a point process ϕ evaluated for a function ν is defined mathematically as the Laplace functional of $-\log \nu$, and is calculated as: $G_\phi(\nu) = \mathbb{E}\left[\prod_{x_i \in \phi} \nu(x_i)\right]$, where the expectation is with respect to ϕ. In our study, the PGF is used for deriving the SINR coverage probability at the typical UE. For this, we derive the PGF of ϕ_S and ϕ_i:

Lemma 2. *The PGF of the stationary, isotropic PLCP ϕ_S is given by:*

$$G_{\phi_S}(\nu) = \exp\left(-2\pi\lambda_R \left(\int_0^\infty 1 - \exp\left(-2\lambda_S \int_0^\infty 1 - \nu\left(\sqrt{r^2+t^2}\right) dt\right)\right) dr\right). \quad (1)$$

The PGF of the PPP ϕ_i, on a randomly oriented line, at a fixed distance d from the origin is:

$$G_{\phi_i,d}(\nu) = \frac{1}{\pi}\int_0^\pi \exp\left(-2\lambda_S \int_0^\infty \left(1 - \nu\left(\left(d^2 + t^2 + 2td\cos\theta\right)^{\frac{1}{2}}\right)\right) dt\right) d\theta. \quad (2)$$

Proof. See Appendix A. □

Let us denote by $G_\phi^x(\nu)$, the conditional PGF of ν with respect to a point process ϕ given that there are no points of the process within a distance x from the origin. This is calculated by changing the lower limit of the outer integral in (1) and the inner integral in (2) from 0 to x. Finally, we note that as the UE compares the powers from the BSs of each tier, it is important to characterize the distance distributions of the nearest points of the PLCP.

Lemma 3. *Let the distance of the nearest point of the PLCP from the origin be given by d_1. Then, the cumulative density*

[2]In point process theory, the Palm probability refers to the probability of an event conditioned on a point of the process being located at a given position.

function (CDF), F_{d_1}, and the probability density function (PDF) of d_1, f_{d_1}, are given by:

$$F_{d_1}(x) = \exp\left(-2\pi\lambda_R\left(x - \int_0^x \exp\left(-2\lambda_S\sqrt{x^2-r^2}\right)dr\right)\right),$$
$$f_{d_1}(x) = 2\pi\lambda_R F_{d_1}(x)\left[2\lambda_S x\int_0^x \frac{\exp(-2\lambda_S\sqrt{x^2-r^2})}{\sqrt{x^2-r^2}}dr\right]. \quad (3)$$

Proof. See Appendix B. □

III. System Model

Consider an urban scenario with a dense blocking environment (see Fig. 1a for an illustration). In this scenario, we study the downlink characteristics of a cellular network consisting of MBS and SBSs. The MBSs operate in the sub-6GHz band, whereas, the multi-RAT SBSs, deployed along the roads (e.g., on the lamp posts [7]), provide high data rate and ad-hoc coverage by jointly exploiting sub-6GHz and mm-wave bands. We assume that the sub-6GHz band is shared by MBSs and SBSs, so that UEs experience both co-tier and cross-tier interference in this band. We study the performance of the pedestrian UEs located on the sidewalks.

A. Network Geometry

The MBS locations are modeled as points of a homogeneous PPP ϕ_M with intensity λ_M defined on $\mathbb{R}^2$. The roads are modeled as realizations of a PLP with intensity λ_R defined on $[0, 2\pi) \times \mathbb{R}^+$. Each road is assumed to contain one sidewalk for pedestrians. The SBSs are deployed on the PLT of the roads and their locations are modeled as the points of a PPP ϕ_i with intensity $\lambda_S \in \mathbb{R}^+$, where i is the index of the road. We denote by ϕ_S the overall SBS process. Furthermore, we consider pedestrian UEs on the sidewalks, whose locations are modeled as an independent stationary PPP ϕ_U along the PLT of roads, with an intensity $\lambda_U \in \mathbb{R}^+$. Accordingly, both the SBSs and UEs are modeled by PLCPs driven by the PLP [22]. Consequently, we have transformed the cellular network considered in our work into a stochastic geometry model as shown in Fig. 1. In Fig. 1, the SBS locations in the same road are modeled by a 1D PPP, and are considered to be neighbors of each other.

B. Static Urban Blockage

For sub-6GHz transmissions from MBSs blockage is generally a secondary effect [23]; moreover, the path-loss exponent calculated from propagation measurements takes the blocking effects into account [24]. Mm-wave transmissions, on the other hand, suffer heavily from blockages and communication becomes infeasible in case the link is blocked. Accordingly, we assume that the power received from a mm-wave SBS whose signal is blocked by a building is null [25].

Due to random blockages, MBSs can be categorized into either LOS or non line-of-sight (NLOS) processes: ϕ_{ML} and ϕ_{MN}, respectively. The intensities of these modified processes are given by $p_M(r)\lambda_M$, and $(1 - p_M(r))\lambda_M$, respectively, where $p_M(r)$ is the probability of an MBS located at a distance r from the UE to be in LOS. In our work, we use the LOS ball approximation [11]. Accordingly, let D_M be the MBS LOS ball radius. The probability of the typical UE to be in LOS from a MBS at a distance r is $p_M(r) = 1$, if $r < D_M$, and $p_M(r) = 0$, otherwise.[3] Furthermore, due to the blockage by buildings, all SBSs in other streets as that of a UE are considered to be in NLOS with respect to that UE (e.g., UE 3 and SBS A in the figure) and are denoted by a process ϕ_{SN}; all SBSs in the same street are denoted by a process ϕ_{SL} and are in LOS (e.g., UE 1 and SBS C) except if vehicles block the signal at cross-roads between the transmitter and the receiver (e.g., UE 2 and SBS B). In our analysis, we use the subscript notation t, v, r, where $t \in \{M, S\}$ denotes the tier (MBS or SBS), $v \in \{L, N\}$ denotes the visibility state, i.e., LOS and NLOS, and $r \in \{\mu, m\}$ denotes the RAT (sub-6GHz or mm-wave). We use the subscript "1" when referring to the *closest* BS of each type. The distance distributions of the nearest BSs of each type and visibility state is given in the following lemma:

Lemma 4. *The distribution of the distance from a UE to the nearest NLOS SBS (d_{SN1}) is given by* (3)*. Whereas, the distributions of the distances from a UE to the closest LOS SBS (d_{SL1}), LOS MBS (d_{ML1}), and NLOS MBS (d_{MN1}) are given by:*

$$f_{d_{SL1}}(x) = 2\lambda_S \exp\left(-2\lambda_S x\right),$$
$$f_{d_{ML1}}(x) = 2\pi\lambda_M x \exp\left(-\pi\lambda_M x^2\right); \quad x < D_M,$$
$$f_{d_{MN1}}(x) = 2\pi\lambda_M x \exp\left(-\pi\lambda_M\left(x^2 - D_M^2\right)\right); \; x \geq D_M, \quad (4)$$

C. Blockage due to Moving Vehicles

We assume that vehicles located on the roads may cause blockage to the mm-wave links. Due to our assumption that the UEs are on the sidewalks, vehicular blockage is caused by vehicles present at crossings of the roads between the UEs and the SBS (see Fig. 1). As the roads are modeled as a Poisson line tessellation (PLT), the number of cross roads between a user and an SBS is Poisson distributed [16], [22]. Accordingly, we evaluate the downlink performance of the typical user by averaging on all the possible blockage conditions by the vehicles present in the crossings. Let the vehicles be of length L_V and relative height h_V with respect to the UE, and located equidistant from each other. Accordingly, if the density of the vehicles is λ_V, the fraction of the roads occupied by the vehicles is $\lambda'_V = L_V \cdot \lambda_V$. As we will see in Section V and VI, the actual mobility model will not play a part in the SINR characterization of the users with instantaneous RAT selection. We plan to consider more realistic mobility models, e.g., Krauss model, General Motors model, or Gipps model [28] in our future work on this subject for evaluating the performance of the average power RAT selection scheme (see Section V-B). Due to the high penetration losses of mm-wave transmissions, we assume that the mm-wave signals are completely lost in case the path between the SBS and

[3]We convert the semi-graded LOS probability model recommended by 3GPP [26] to a step probability model, following criterion 1 in [27].

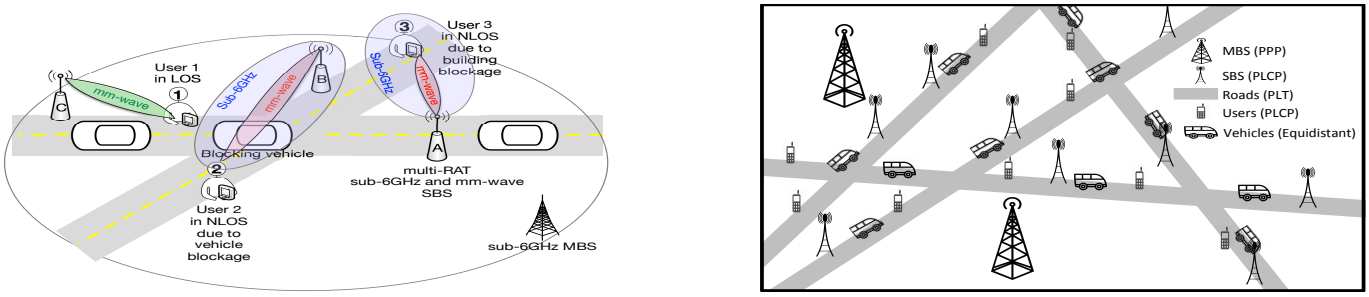

(a) (b)

Fig. 1. (a) System model showing on-road deployment of SBSs with pedestrian UEs, and (b) Different point processes in the stochastic geometry model of the network under investigation.

the UE is obstructed by a vehicle [25].[4] Although mm-waves can provide very high throughputs, the blockage due to vehicles can be detrimental for services requiring a high reliability. Note that although secondary paths may exist for mm-wave propagation due to specular reflections, we assume that reflected signals contribute insignificantly to the received power. It must be noted that in certain deployment topologies NLOS communication in dense urban environments is indeed viable [29]. In fact, measurements show that in case of small incidence angles and reflections from materials such as tainted windows, significant received power exists. However, in our urban cellular network, not only the incidence angles are large (it is small only when the UE, the blocking vehicle, and the BS are arbitrarily close to each other, which is unrealistic), but also reflected power is obtained from the sidelobe transmissions (i.e., we do not assume the switching of the beam direction to a secondary reflected path to facilitate NLOS communication). Additionally, the reflective surfaces encountered in an urban scenario are typical outdoor building materials like brick walls, which are very poor reflective surfaces [30]. As a consequence, we assume in our work that mm-wave communication is infeasible using NLOS links. We will treat the NLOS mode of operation in our system in a future work.

D. Path Gain

The path-gain at a distance d_{tvr} from a transmitter is given by $h_r K_r d_{tvr}^{-\alpha_{tvr}}$, where K_r and α_{tvr} are the path-loss coefficient and exponent, respectively. For sub-6GHz communications, we assume a Rayleigh fast fading h_μ, with unit variance. Whereas, due to the low local scattering, we consider a Nakagami fading h_m with shape factor n_0 for mm-wave communications [23]. In our work, we assume a sectored model for the transmission pattern of the mm-wave antennas [11], consisting of a main-lobe of beamwidth θ, and a side-lobe. Let G_0 be the directivity gain product of the main-lobe transmitting and receiving antenna[5]; then, the received power at a distance d_{tvr} is given by $P_{tv\mu} = P_t h_\mu K_\mu d_{tv\mu}^{-\alpha_{tv\mu}}$ for sub-6GHz and $P_{tvm} = G_0 P_t h_m K_m d_{tvm}^{-\alpha_{tvm}}$ for mm-wave transmissions, where P_t is the transmit power of a BS of tier t. Following our observations on mm-wave blockage for NLOS SBS, we have, $P_{SNm} = 0$.

E. Tier and RAT Selection Procedure

We assume that the UEs are uniformly distributed along the roads, and associate to the BS providing the maximum downlink received power. For this, the BSs send their control signals in the sub-6GHz band, which is more reliable as compared to the mm-wave band. A UE may select mm-wave RAT when the strongest BS is an SBS. In this case, it compares the power in sub-6GHz band (i.e., $P_S h_\mu K_\mu d_{Sv\mu}^{-\alpha_{Sv\mu}}$) with that in the mm-wave band biased by a multiplicative factor Q_R (i.e., $Q_R G_0 P_t h_m K_m d_{tvm}^{-\alpha_{Svm}}$). Let us recall that in our system model, the network slices are realized by partitioning of the available network resources, thereby enabling creation of virtual parallel networks. The users attach to one of the slices provided by the network operator using information exchanged in the control channel during the association phase. Then, depending on the associated slice, a corresponding value of Q_R is utilized for RAT selection. The parameter Q_R is called the RAT selection bias and will be used to differentiate the network slices.

The power in each band can be either measured instantaneously, or averaged over a time window. In the *instantaneous power RAT selection* case, the UE simultaneously measures the mm-wave power received in different control channels and averages out the effect of fast fading. The instantaneous vehicular blockage condition may however inhibit a proper RAT selection. When *averaged power RAT selection* is performed, the UE measures the mm-wave power for a longer duration of time attempting to average out the effect of the vehicular blockages as well, which gives a more accurate idea of the radio scene. In our analysis we will compare the mm-wave selection probability of both these schemes.

Finally, the way the parameter Q_R should be optimized is highly dependent on the QoS requirements of each slice. We thus assume that the UEs are connected to a slice characterized by QoS triplets $T^* = (\mathcal{B}^*, \mathcal{P}_C^*, \mathcal{P}_R^*)$, where $\mathcal{B}^*$ is the tolerable vehicular blockage probability, $\mathcal{P}_C^*$ is the minimum SINR coverage probability, and $\mathcal{P}_R^*$ is the target rate coverage. It must be noted that URLLC applications are typically characterized by very stringent delay and outage

[4]Thanks to multi-path propagation and larger beam-widths, which result in larger angular spread for the signal, we assume that the vehicular blockages do not affect the sub-6GHz band communications significantly.

[5]For highly directional antennas, the side-lobe gain is negligible; thus, for simplicity, we assume it to be zero.

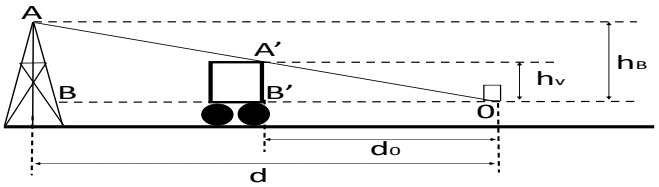

Fig. 2. Model for calculating the blockage due to moving vehicles.

requirements [31]. The vehicular blockage probability in our work can be easily mapped to the classical reliability metric of URLLC performance. As an example, given a vehicular blockage probability of B^*, the users in the network connected to mm-wave RAT will not be able to experience a SINR coverage higher than $1 - B^*$.

Similarly, by controlling the mm-wave link blockage experienced by the users, the operator can provide performance guarantee on the violation of latency constraints of URLLC applications. As an example, let us assume a typical C-segment medium sized cars, with $h_V = 4.5$ m and $L_V = 1.5$ m [32]. If a vehicle is moving with a speed of 80 km per hour, then the user commencing an NLOS regime due to vehicular blockage, will experience a link blockage of 67.5 ms (obviously, this value changes with the size and the speed of the vehicles). Let us recall that the packet deadline for URLLC applications can be much lower than a few ms [33]. As a result, in case a user running a URLLC application observes that its communication link state has changed to outage state, the latency constraint of the application is violated with probability 1. Thus, in case the vehicular blockage probability is B, the probability that the latency constraint of a URLLC application is violated is given by B.

The vehicular blockage probability experienced by the users depends on the selected RAT in our system model, which can be controlled by the choice of Q_R. However, it must be noted that in a real-world system incorporating network slicing, only tuning Q_R to satisfy the QoS requirements of the services is inadequate, and obviously, it will depend on multiple other parameters.

IV. Vehicular Blockage and mm-wave Interference

In this section, we derive the vehicular blockage probability, and we propose an interference model for system-level evaluations of mm-wave networks.

A. Characterization of the Vehicular Blockage Probability

We study the blockages of the link between the SBSs and the UEs due to the vehicles (see Fig. 2), and use this result to derive the mm-wave selection probability and the overall SINR.

Proposition 1. *The probability that a link between an SBS and a UE at a distance d is not blocked by a vehicle is given by: $\mathcal{L}(d) = \exp\left(-\lambda'_V \lambda_R \frac{h_V}{h_B} d\right)$, where h_B is the relative height of the SBS with respect to the UE. Thus, the vehicular blockage probability $\mathcal{B}(Q_R)$, i.e., the probability given Q_R that a UE served in the mm-wave RAT is blocked by a vehicle is given by:*

$$\mathcal{B}(Q_R) = \int_0^H \left(1 - \exp\left(-\lambda_R \lambda'_V \frac{h_V}{h_B} x\right)\right) f_{d_{SL1}}(x) dx, \tag{5}$$

where the upper limit in the integral is given by $H = \left(\frac{K_m G_0 Q_R}{K_\mu}\right)^{\frac{1}{\alpha_{SLm} - \alpha_{SL\mu}}}$.

Proof. See Appendix C. □

B. Interference Characterization in mm-Wave

Interference models traditionally used in the stochastic geometry literature are planar and thus ignore the elevation of the antenna pattern. In this section, we propose a model to overcome this limitation in a tractable way for accurately analyzing a scenario where the SBSs are deployed along a road. For this, we first characterize the interference caused by an SBS to a UE served by its n-th neighboring SBS of the same street. Observe that the SBS to which a UE U is associated (SBS 1 in Fig. 3a), causes interference to UEs located in the n-th neighboring SBS if its beam reaches (at location X on the figure) the n-th cell. As a worst case interference scenario, assume 1) that U is located at cell boundary (at distance $\frac{d_a}{2}$ from the SBS, where d_a is the distance between SBSs 1 and 2) and 2) that this interfering signal is not obstructed by any vehicle.

Lemma 5. *In the worst case scenario, the probability that an SBS causes interference in mm-wave transmissions in the coverage area of its n-th neighbor is given by:*

$$\mathcal{P}_{n,WC} = \mathbb{E}_{d_{n-1},d_n}\left[\exp\left(-2\lambda_S h_B \frac{d_n + d_{n-1} - 2h_B \tan\frac{\theta}{2}}{2h_B + (d_n + d_{n-1})\tan\frac{\theta}{2}}\right)\right], \tag{6}$$

where d_n and d_{n-1} are the distances between the serving SBS and the n-th and (n-1)-th neighboring SBS, respectively, and θ is the beamwidth. The expectation is with respect to the joint distribution of d_n and d_{n-1}, which is given by $f_{d_{n-1},d_n}(x,y) = \frac{\lambda_S^2 \exp(-\lambda_S y)}{(n-2)!}(\lambda_S x)^{n-2}$, for $y \geq x$.

Proof. See Appendix D. □

In the general case, the accurate characterization of the actual interference is relatively difficult, precisely due to two reasons: 1) the position distributions of the served UEs for each SBS up to the n-th SBS should be taken into account, and 2) in the presence of vehicular blockages, the number of neighboring blocked SBSs that do not contribute to the interference, is a random variable. Moreover, our results in Section VIII suggest that the dominant-interferer contributes to almost all the interference. Our model is thus based on the following assumption.

Assumption 1. *The closest SBS on the same sidewalk on which the serving SBS is located, along the ray joining the serving SBS and the user, i.e., the dominant-interferer, is the only SBS that creates substantial interference to the UEs in*

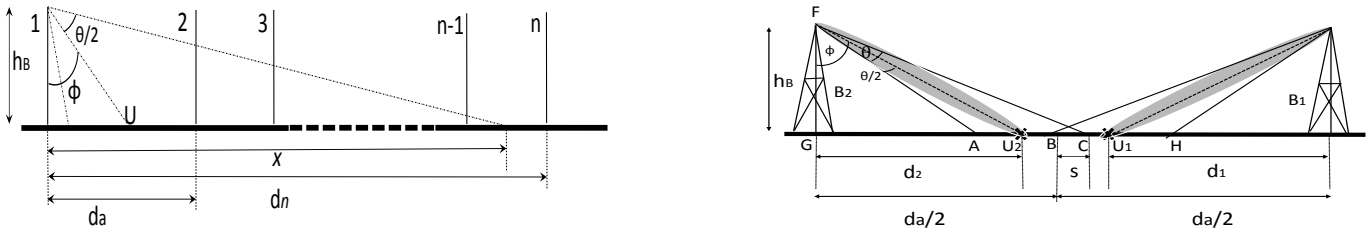

(a) (b)

Fig. 3. (a) Interference to the n-th SBS from the typical SBS, and (b) Simplified interference model for LOS mm-wave SBS.

mm-wave. Accordingly, if the dominant-interferer is blocked, the mm-wave transmission is noise-limited.

Based on this assumption, we compute the probability $\bar{p}_G$ that the dominant-interferer creates interference to the typical UE, in case it is not blocked by a vehicle. As shown in Fig. 3b, the dominant-interferer B_2 causes interference if its beam partly overlaps the coverage of SBS B_1.

Lemma 6. *For an arbitrary small beamwidth θ, the typical UE experiences mm-wave interference from its closest neighboring SBS with a probability ($\bar{p}_G$) given by* (7)*, where* $x_0 = 2h_B \tan\left(\frac{\theta}{2}\right)$, $x_1 = h_B \tan\left(\arctan\frac{x}{2h_B} - \frac{\theta}{2}\right)$, $x_2 = h_B \tan\left(\arctan\left(\frac{x}{h_B}\right) - \frac{\theta}{2}\right)$, *and* $f_{xy}(x,y) = \lambda_S\lambda_U \exp(-\lambda_S x)\exp\left(-\lambda_U\left(\frac{x}{2}-y\right)\right)$.

Proof. See Appendix E. □

The condition on the beamwidth comes from the simplifying assumption that the spillover created by the SBS B_2 by serving a UE U_2 in its neighboring cell B_1 does not go beyond B_1[6].

This model has the advantage of being tractable for system level evaluations. It also provides more accurate results than a noise-limited approach (see Section VIII).

V. Association Probabilities

In this section, we derive the BS tier selection probabilities and the RAT selection probabilities for mm-wave and sub-6GHz bands.

A. Tier Selection for a UE

For each UE, there are four cases for the serving BS: MBS in LOS (ML), MBS in NLOS (MN), SBS in LOS (SL), and SBS in NLOS (SN). Let E_{tv} denote the event that the serving BS is of tier $t \in \{M, S\}$ and in visibility state $v \in \{L, N\}$. In what follows, we describe the association probabilities for the case where $\{tv\} = \{ML\}$. Note that for E_{ML}, we only have to consider the joint event $\{P_{ML1} > P_{SL1}\} \cap \{P_{ML1} > P_{SN1}\}$ as in our model we always have $P_{ML1} > P_{MN1}$. This event can occur in two ways: (i) $P_{ML1} > P_{SL1} > P_{SN1}$, or (ii) $P_{ML1} > P_{SN1} > P_{SL1}$. For the first event (i):

$$P_{ML1} > P_{SL1} > P_{SN1} \iff$$

$$\left(\frac{P_S}{P_M} d_{ML1}^{\alpha_{ML\mu}}\right)^{\frac{1}{\alpha_{SL\mu}}} < d_{SL1} < d_{SN1}^{\frac{\alpha_{SN\mu}}{\alpha_{SL\mu}}}.$$

Using the CDF of d_{SL1} (see Lemma 4), for given instances of d_{ML1} and d_{SN1}, we have:

$$\mathbb{P}\left(\left(\frac{P_S}{P_M} d_{ML1}^{\alpha_{ML\mu}}\right)^{\frac{1}{\alpha_{SL\mu}}} < d_{SL1} < d_{SN1}^{\frac{\alpha_{SN\mu}}{\alpha_{SL\mu}}} \mid d_{ML1}, d_{SN1}\right) = \exp\left(-2\lambda_S\left(d_{SN1}^{\frac{\alpha_{SN\mu}}{\alpha_{SL\mu}}} - \left(\frac{P_S}{P_M} d_{ML1}^{\alpha_{ML\mu}}\right)^{\frac{1}{\alpha_{SL\mu}}}\right)\right) \cdot \exp\left(-2\lambda_S\left(\left(\frac{P_S}{P_M} x^{\alpha_{ML\mu}}\right)^{\frac{1}{\alpha_{SL\mu}}}\right)\right).$$

Then, taking the expectations with respect to d_{ML1} and d_{SN1} (see Lemmas 3 and 4), we evaluate the probability of (i). Similarly, we can evaluate the probability of the event (ii), where in the first step, we use the CDF of the variable d_{SN1}, and then we take expectations with respect to d_{ML1} and d_{SL1}. Finally, to compute the overall ML association probability, the sum of the probabilities of (i) and (ii) is multiplied with the probability that there exists a LOS MBS, i.e., $W_1 = 1 - \exp\left(-\pi\lambda D_M^2\right)$. In a similar manner, all the other probabilities are calculated.

Proposition 2. *The probabilities of association of a UE with a LOS and NLOS MBS and LOS SBS are given by* (8)*, where:* $W_1 = 1 - \exp\left(-\pi\lambda_M D_M^2\right)$, $\mathcal{T}_1(x) = \exp\left(-2\lambda_S\left(\left(\frac{P_S}{P_M} x^{\alpha_{ML\mu}}\right)^{\frac{1}{\alpha_{SL\mu}}}\right)\right)$, $\mathcal{T}_2(x) = \exp\left(-2\lambda_S\left(\frac{P_S}{P_M} x^{\alpha_{MN\mu}}\right)^{\frac{1}{\alpha_{SL\mu}}}\right)$, *and* $\mathcal{T}_3(x) = \exp\left(-\pi\lambda_M\left(\left(\frac{P_M}{P_S} x^{\alpha_{SL\mu}}\right)^{\frac{1}{\alpha_{MN\mu}}}\right)\right)$. *$F_{d_{SN1}}(x)$ refers to the CDF of the first NLOS SBS, as given by Lemma 3.*

Proof. See Appendix F. □

We now derive the distribution of the distance between a UE and its associated serving BS.

Lemma 7. *Given that a UE is associated to a BS of a tier t with visibility state v, the PDF of its distance from the serving BS is given by:*

$$\hat{f}_{d_{tv1}}(x) = \frac{f_{d_{tv1}}(x)}{\mathcal{P}_{tv}} \prod_{\forall (t'v' \neq tv)} \mathbb{P}(\phi_{t'v'} \cap (0,x) = 0), \quad (9)$$

[6]For a given θ, this occurs with a probability $\exp(\frac{h_B}{2\tan(\frac{\theta}{2})}\sqrt{1-\tan^2(\frac{\theta}{2})})$, which tends to 1 as $\theta \to 0$. In deterministic deployments, an operator can set $\theta \leq 2\arctan(\frac{h_B d_a}{2h_B^2 + d_a^2})$ to ensure that this condition always holds.

$$\bar{p}_G = \int_{x_0}^{\infty}\int_{x_1}^{x_2} \exp\left(-\lambda_S\left(x - h_B\tan\left(\frac{\theta}{2} + \arctan\frac{y}{h_B}\right)\right)\right)\left(1-\exp\left(\lambda_U\left(\frac{x}{2}-x_1\right)\right)\right) f_{yx}(y,x)dydx + \int_{x_0}^{\infty}\int_{x_2}^{\frac{x}{2}} \left(1-\exp\left(\lambda_U\left(\frac{x}{2}-x_1\right)\right)\right) f_{yx}(y,x)dydx. \quad (7)$$

$$\mathcal{P}_{ML} = W_1\left(\int_0^{\infty}\int_x^{\infty}\exp\left(-2\lambda_S\left(y^{\frac{\alpha_{SN\mu}}{\alpha_{SL\mu}}} - \left(\frac{P_S}{P_M}x^{\alpha_{ML\mu}}\right)^{\frac{1}{\alpha_{SL\mu}}}\right)\right)\mathcal{T}_1(x) f_{d_{SN1}}(y) f_{d_{ML1}}(x)dydx + \int_0^{\infty}\int_0^{x}\left(F_{d_{SN1}}\left(x^{\frac{\alpha_{SL\mu}}{\alpha_{SN\mu}}}\right) - F_{d_{SN1}}\left(\left(\frac{P_S}{P_M}y^{\alpha_{ML\mu}}\right)^{\frac{1}{\alpha_{SN\mu}}}\right)\right) F_{d_{SN1}}\left(x^{\frac{\alpha_{SL\mu}}{\alpha_{SN\mu}}}\right) f_{d_{ML1}}(y) f_{d_{SL1}}(x)dydx\right). \quad (8a)$$

$$\mathcal{P}_{MN} = (1-W_1)\left(\int_0^{\infty}\int_0^{x}\exp\left(-2\lambda_S\left(y^{\frac{\alpha_{SN\mu}}{\alpha_{SL\mu}}} - \left(\frac{P_S}{P_M}x^{\alpha_{MN\mu}}\right)^{\frac{1}{\alpha_{SL\mu}}}\right)\right)\mathcal{T}_2(x) f_{d_{SN1}}(y) f_{d_{MN1}}(x)dydx + \int_0^{\infty}\int_x^{\infty}\left(F_{d_{SN1}}\left(x^{\frac{\alpha_{SL\mu}}{\alpha_{SN\mu}}}\right) - F_{d_{SN1}}\left(\left(\frac{P_S}{P_M}y^{\alpha_{MN\mu}}\right)^{\frac{1}{\alpha_{SN\mu}}}\right) F_{d_{SN1}}\left(x^{\frac{\alpha_{SL\mu}}{\alpha_{SN\mu}}}\right)\right) f_{d_{MN1}}(y) f_{d_{SL1}}(x)dydx\right). \quad (8b)$$

$$\mathcal{P}_{SL} = W_1\left(\int_0^{\infty}\int_x^{\infty}\exp\left(-\pi\lambda_M\left(\left(\frac{P_M}{P_S}y^{\alpha_{SN\mu}}\right)^{\frac{1}{\alpha_{ML\mu}}} - \left(\frac{P_M}{P_S}x^{\alpha_{SL\mu}}\right)^{\frac{1}{\alpha_{ML\mu}}}\right)\right)\mathcal{T}_2(x) f_{d_{SL1}}(x) f_{d_{SN1}}(y)dydx + \int_0^{\infty}\int_0^{x}\left(F_{d_{SN1}}\left(\left(\frac{P_S}{P_M}x^{\alpha_{ML\mu}}\right)^{\frac{1}{\alpha_{SN\mu}}}\right) - F_{d_{SN1}}\left(y^{\frac{\alpha_{SL\mu}}{\alpha_{SN\mu}}}\right) F_{d_{SN1}}\left(\left(\frac{P_S}{P_M}x^{\alpha_{ML\mu}}\right)^{\frac{1}{\alpha_{SN\mu}}}\right)\right) f_{d_{SL1}}(y) f_{d_{ML1}}(x)dydx\right) + (1-W_1)\left(\int_0^{\infty}\int_x^{\infty}\exp\left(-\pi\lambda_M\left(\left(\frac{P_M}{P_S}y^{\alpha_{SN\mu}}\right)^{\frac{1}{\alpha_{MN\mu}}} - \left(\frac{P_M}{P_S}x^{\alpha_{SL\mu}}\right)^{\frac{1}{\alpha_{MN\mu}}}\right)\right)\mathcal{T}_3(x)\ f_{d_{SL1}}(x) f_{d_{SN1}}(y)dydx + \int_0^{\infty}\int_0^{x}\left(F_{d_{SN1}}\left(\left(\frac{P_S}{P_M}x^{\alpha_{ML\mu}}\right)^{\frac{1}{\alpha_{SN\mu}}}\right) - F_{d_{SN1}}\left(y^{\frac{\alpha_{SL\mu}}{\alpha_{SN\mu}}}\right) F_{d_{SN1}}\left(\left(\frac{P_S}{P_M}x^{\alpha_{ML\mu}}\right)^{\frac{1}{\alpha_{SN\mu}}}\right)\right) f_{d_{SL1}}(y) f_{d_{MN1}}(x)dydx\right). \quad (8c)$$

$$\mathcal{P}_{SN} = 1 - \mathcal{P}_{ML} - \mathcal{P}_{MN} - \mathcal{P}_{SL} \quad (8d)$$

where $f_{d_{tv1}}(x)$ is the PDF of the distance of the nearest BS of type tv, $t \in \{M,S\}$ and $v \in \{L,N\}$, as derived in (4)*.*

B. RAT Selection for Pedestrian UE

After having selected an SBS as the serving BS, a UE shall select the serving RAT. Here we recall that depending on the network slice with which the user is associated to, the value of the RAT selection bias Q_R varies. Specifically, using the slice-dependent RAT selection bias, the users select either the sub-6GHz RAT or the mm-wave RAT. We thus derive and analyze the mm-wave selection probabilities for 1) the instantaneous power RAT selection scheme and 2) the averaged power RAT selection scheme described in Section III-E.

Proposition 3. *The conditional mm-wave selection probability, given that the UE is associated with an LOS SBS and use instantaneous power RAT selection is given by:*

$$\mathcal{P}_m = \frac{2h_B\lambda_S}{\lambda'_V h_V \lambda_R + 2h_B\lambda_S}\cdot \left[1-\exp\left(-2\lambda_S\left(\frac{K_m G_0 Q_R}{K_\mu}\right)^{\frac{1}{\alpha_{SLm}-\alpha_{SL\mu}}}\right)\right]. \quad (10)$$

In case the UE selects the RAT by adopting the averaged power RAT selection scheme, the mm-wave selection probability is given by:

$$\bar{\mathcal{P}}_m = \exp\left(\frac{-2\lambda_S h_B\left(\alpha_{SLm}-\alpha_{SL\mu}\right)}{\lambda'_V\lambda_S h_V}\ \mathcal{W}\left(\frac{\lambda'_V\lambda_S h_v}{h_B\left(\alpha_{SLm}-\alpha_{SL\mu}\right)}\left(\frac{K_m G_0 Q_R}{K_\mu}\right)^{\frac{1}{\alpha_{SLm}-\alpha_{SL\mu}}}\right)\right). \quad (11)$$

where $\mathcal{W}$ is the Lambert W-Function.

Proof. See Appendix G. □

From this lemma, some immediate observations follow as given below.

Remark 1. *From* (10)*, we observe that the mm-wave selection probability in case of instantaneous power RAT selection is upper bounded by $\mathcal{P}^*_m = \frac{2h_B\lambda_S}{\lambda'_V h_V\lambda_R + 2h_B\lambda_S}$, regardless of G_0 or Q_R. From* (11)*, we observe that with averaged power scheme, it is possible to have a greater degree of RAT tunability (because $\bar{\mathcal{P}}_m \to 1$ as $Q_R \to \infty$ or $G_0 \to \infty$).*

The overall association probability of the typical UE is given by $\mathcal{P}_{tvr} = \mathcal{P}_{tv}\mathcal{P}_r$, where, $r \in \{S,M\}$, $v \in \{L,N\}$, and $r \in \{\mu, m\}$. When the serving BS is not a LOS SBS, as we have exclusively sub-6GHz operation ($r = \mu$), it follows that $\mathcal{P}_m = \bar{\mathcal{P}}_m = 0\ \forall\{t,v\} \neq \{S,L\}$.

VI. SINR Coverage Probabilities

In this section, we derive the downlink SINR coverage probability of the typical UE, which is mathematically defined as $\mathcal{P}_C(\gamma) = \mathbb{P}(SINR > \gamma)$. Following the theorem of total probabilities:

$$\mathcal{P}_C(\gamma) = \sum_{t\in\{M,S\},\, v\in\{L,N\},\, r\in\{\mu,m\}} \mathbb{P}(SINR_{tvr} > \gamma | t,v,r)\mathcal{P}_{tvr}. \tag{12}$$

In case of mm-wave association, we provide a lower bound of the SINR coverage probability, which we show to be tight in Section VIII-A.

Theorem 1. *The conditional SINR coverage probability, given that the typical UE is associated to a BS of type 'tv' in sub-6GHz is given by:*

$$\mathbb{P}\left(SINR_{tv\mu} \geq \gamma\right) = \mathbb{E}_{d_{tv1}}\left[\exp\left(-\frac{\gamma\sigma_\mu^2}{P_S K_\mu d_{tv1}^{-\alpha_{SL\mu}}}\right)\right.$$
$$\prod_{\substack{\{t'v'\}\\ \neq\{tv\}}} G_{\phi_{t'v'}}^{\tilde{d}_{tv}}\left(\frac{P_{t'}x^{\alpha_{t'v'}}}{P_{t'}x^{\alpha_{t'v'}} + \gamma P_t d_{tv1}^{\alpha_{tv}}}\right) \cdot$$
$$\left. G_{\phi_{i,d_{SN1}}}^{\tilde{d}_{tv}}\left(\frac{\gamma d_{S1}^{\alpha_{SN\mu}}}{x^{\alpha_{SN\mu}} + \gamma d_{S1}^{\alpha_{SN\mu}}}\right) G_{\phi_{tv}\setminus\{tv1\}}^{d_{tv1}}\left(\frac{x^{\alpha_{tv}}}{x^{\alpha_{tv}} + \gamma d_{tv1}^{\alpha_{tv}}}\right)\right]. \tag{13}$$

For NLOS SBS association, i.e., $t = S$ and $v = N$, the term $G_{\phi_{i,d_{SN1}}}^{\tilde{d}_{tv}}(\cdot)$ is replaced by $G_{\phi_{i,d_{S1}}\setminus\{SN1\}}^{\tilde{d}_{tv}}(\cdot)$. The PGFs of the NLOS SBS process are given in Lemma 2. For the PGF of the MBS and LOS SBS processes, see [22]. The conditional SINR coverage probability, given that the typical UE is associated to a SBS in mm-wave is lower bounded by:

$$\mathbb{P}\left(SINR_{SLm} \geq \gamma\right) \geq \sum_{n=1}^{n_0} (-1)^{n+1}\binom{n_0}{n}$$
$$\mathbb{E}_{d_{SL1},d_{SL2}}\left[\exp\left(-n\gamma_0 d_{SL1}^{-\alpha_{SLm}}\exp\left(K_0 d_{SL1}\right)\right)\right.$$
$$\left.\frac{\exp\left(-K_0 d_{SL1}\right) d_{SL1}^{-2}}{\exp\left(-K_0 d_{SL1}\right) d_{SL1}^{-2} + n\gamma p_G \exp\left(-K_0 d_{SL2}\right) d_{SL2}^{-2}}\right], \tag{14}$$

where $K_0 = \lambda_R \lambda'_V \frac{h_V}{h_B}$, $\tilde{d}_{tv} = \left(\frac{P_{t'}}{P_t} d_{tv1}^{\alpha_{tv1}}\right)^{\frac{1}{\alpha_{t'v'1}}}$, and the expectation is taken with respect to the joint distribution of d_{SL1} and d_{SL2}: $f_{d_{SL2},d_{SL1}}(x,y) = 2\lambda_S^2 \exp(-\lambda_S(x+y))$.

Proof. See Appendix H. □

Once the SINR coverage probability is obtained, the rate coverage probability for each tier and RAT is computed as: $\mathcal{P}_{Rtvr}(r_0) = \mathbb{P}\left(SINR_{tvr} \geq 2^{\frac{r_0}{B}} - 1\right) = \mathbb{P}_{Ctvr}\left(2^{\frac{r_0}{B_r}} - 1\right)$. Consequently, the overall rate coverage probability follows from the theorem of total probabilities:

$$\mathcal{P}_R(r_0) = \sum_{t\in\{M,S\},\, v\in\{L,N\},\, r\in\{\mu,m\}} \mathbb{P}(SINR_{tvr} > 2^{\frac{r_0}{B_r}} - 1 | t,v,r)\mathcal{P}_{tvr}. \tag{15}$$

VII. A Slice-Aware RAT Selection Mechanism

A. Effect of RAT Selection Bias on Blockage, SINR, and Rate

We analyze the RAT selection from the perspective of three services [21]: i) URLLC characterized by tight link blockage requirement and high SINR coverage constraint, ii) mMTC characterized by continuous and ubiquitous coverage requirement and less stringent blockage constraints, and iii) eMBB characterized by high data rate requirement, under coverage constraints. In this section, we highlight the impact of the RAT selection probability on the blockage, SINR, and data rate. We then propose a slice-aware RAT selection strategy for the three services.

1) Effect of Bias on Blockage: For blockage-sensitive UEs, Q_R should be such that the vehicular blockage probability given that a UE is served in mm-wave band (5) is limited.

Remark 2. *From* (5)*, we observe that $\mathcal{B}(Q_R)$ increases with Q_R, and thus, for a given λ_S, there exists a maximum value of Q_R, beyond which the vehicular blockages become unacceptable. As $Q_R \to \infty$, the vehicular blockage probability, $\mathcal{B}(Q_R)$, attains a value $1 - \mathcal{P}_m^*$, where $\mathcal{P}_m^*$ is the maximum mm-wave selection probability given in Remark 1.*

Corollary 1. *Leveraging on Remark 2, the minimum SBS deployment density that guarantees the vehicular blockage probability to be less than $\mathcal{B}^*$, regardless of the RAT biasing is:*

$$\lambda_S^* = \frac{(1-\mathcal{B}^*)}{2\mathcal{B}^*}\lambda_R \lambda'_V \frac{h_V}{h_B}. \tag{16}$$

This enables the operator to properly dimension the cellular network, in terms of the minimum deployment density of SBS, so as to ensure reliable mm-wave service.

2) Effect of Bias on SINR and Data Rate: As we will show in Section VIII-C, for a given λ_S, the SINR and rate coverage probability can either decrease or increase, depending on λ_V. In some cases, a non-trivial optimal RAT selection bias exists. This optimal RAT bias values (distinct for SINR and rate) can be obtained using a random-restart hill climbing algorithm [6].

B. Protocol for Slice-Aware RAT Selection

In our system model, the service requirements are characterized by a maximum tolerable vehicular blockage probability, a minimum SINR coverage probability, and a target rate coverage probability. As observed in Remark 2, Q_R can take values between 0 dB and a maximum value (say Q_B), which depends on λ_V. On the other hand, let the range of bias values that satisfy the SINR coverage probability constraint be given by (Q_{C1}, Q_{C2}). Similarly, let the bias range that satisfies a target rate coverage probability be given by (Q_{R1}, Q_{R2}).

We assume that for the QoS requirements of different slices, the network calculates the slice specific bias ranges $(1, Q_B)$, (Q_{C1}, Q_{C2}), and (Q_{R1}, Q_{R2}). For a given slice, and the associated bias range, the network computes and broadcasts the optimal bias value (Q_R^*), which in case of URLLC and mMTC services maximizes the SINR coverage, and in case of eMBB maximizes the data rate. Note that in our framework, we have assumed that the optimization objective for both the URLLC and the mMTC applications is SINR coverage. However, as the URLLC applications are typically characterized by very high reliability in the communication links, the mm-wave selectivity for URLLC application is very limited. As a result, we will see in Section VIII-D, the domain of the allowable bias values

are quite different for the two applications specifically due to difference in the allowable vehicular blockages. Accordingly, the degree of mm-wave selection probability is dramatically different for the two applications (see Section III-E for a discussion on how the vehicular blockage probability can be mapped to classical QoS parameters for URLLC applications, e.g., reliability in terms of outage and a bound on the violation of latency constraints of the application. Q_R^* is obtained using a random restart hill-climbing algorithm [6] such that $Q_R^* \in (1, Q_B) \cap (Q_{C1}, Q_{C2}) \cap (Q_{R1}, Q_{R2})$. When a UE associates to an SBS, it receives the bias value depending on its slice and uses it for the RAT selection procedure. In the next section, we will show how the mm-wave association probability varies for the three types of slice. In Algorithms 1 and 2, we summarize our RAT selection strategies at network and UE sides, respectively.

VIII. Numerical Results

Here, we provide some numerical results to reveal the salient characteristics of the network. First, we validate our analytical model using Monte-Carlo simulations for evaluating numerically the downlink SINR. For that, we generate the PPP distributed MBSs, the PLCP based SBSs, and the users [22]. Then following the max-power based tier selection procedure, the instantaneous RAT selection is evaluated by a simple probability based assumption, i.e., the probability of having a LOS link is $1 - \lambda_V$ (see Section V-B). We assume a MBS deployment density of $\lambda_M = 5$ km^{-2}, and transmit powers $P_S = 30$ dBm and $P_M = 45$ dBm. N_0 is assumed to be -174 dBm/Hz and the operating frequencies are 2.3 GHz and 60 GHz for sub-6GHz band and the mm-wave band, respectively, with the corresponding bandwidths being 20 MHz and 1 GHz. The Nakagami parameter is assumed to be $n_0 = 3$, the antenna beamwidth is assumed to be $\theta = 10°$, and the relative height of the SBSs is assumed to be $h_B = 10$ m. The path-loss parameters are derived from 3GPP reports [24], [34]. Finally, regarding the vehicles, we assume C-segment medium sized cars, with $h_V = 4.5$ m and $L_V = 1.5$ m [32].

A. Validation of the mm-wave Interference and SINR Model

In Fig. 4a, we compare the analytical SINR coverage probability (see Theorem 1) with Monte Carlo simulations[7]. We observe that the analytical results agree with the simulations. Specifically, for $G_0 = 35$ dBi, we see that the lower bound of Theorem 1 is very tight. In Fig. 4b, we use simulations to compare the SINR coverage with only noise, only the dominant-interferer (see Assumption 1), or the whole interference. We see that our dominant-interferer model is accurate to represent interference in mm-wave and that the noise limited model is unacceptable. Accordingly, we rely on the analytical model developed in this paper to study the performance trends of the network.

[7]The final integral of (3) does not have a closed form. We simplify the evaluation by expanding the exponential term in the numerator, i.e., $\exp(-2\lambda_S\sqrt{x^2 - r^2})$, with a power series, and evaluating each of the resulting integral terms separately.

B. Association and RAT Selection Probabilities

In Fig. 4c, we plot the association probabilities for pedestrian UEs (see Proposition 2). As expected, as λ_S increases for a given λ_R, the LOS SBS association probability increases and the MBS association probability decreases. However, with increasing λ_S, the NLOS SBS association is fairly negligible except for very high road densities (e.g., $\lambda_R = 15$ km^{-1}). In Fig. 5a, we plot the mm-wave selection probability with the *instantaneous power RAT selection* with respect to Q_R, given that the typical UE has selected an LOS SBS (Proposition 3). Increasing either or both Q_R and G_0 facilitates an increase in mm-wave RAT selection. More interestingly, G_0 has a more pronounced effect on mm-wave selection than increasing λ_S. For example, with $G_0 = 10$ dBi and $Q_R = 24$ dB, doubling λ_S from 5 to 10 km^{-1} increases the mm-wave selection from 50% to 70%, whereas, setting $G_0 = 20$ dBi ensures 100% mm-wave RAT selection. Thus, an operator requiring aggressive mm-wave selection may prefer to invest in more efficient antennas rather than increasing λ_S. Following Remark 1, we observe that with the *instantaneous power RAT selection*, in the presence of vehicles, $\mathcal{P}_m$ saturates to a value less than 1. On the contrary, the *averaged power RAT selection* (see Lemma 3) has a greater RAT tunability (as shown in Fig. 5b), and enables to increase the mm-wave selection probability. However, increased measurement duration may lead to higher access delay, which is a tradeoff we aim to study in future works. In the following, we perform our analysis using the instantaneous power RAT selection.

C. SINR Coverage Probabilities

In Fig. 6a, we plot the SINR coverage probability (Theorem 1). With $G_0 = 10$ dBi and $Q_R = 0$ dB, in case of LOS SBS association, the UE always selects sub-6GHz RAT. Moreover, we observe that increasing λ_R slightly decreases the SINR performance because the sub-6GHz interference increases. In the same way, the SINR enhancement in the sub-6GHz band achieved by increasing λ_S is fairly limited. In Fig. 6b, we plot the SINR coverage probability with respect to λ_S with fixed G_0 and Q_R to accurately observe this trend. For UEs operating only in sub-6GHz band, it may not be possible to maintain a desired SINR coverage in cities with dense roads by simply increasing λ_S. This is because a UE perceives higher LOS interference, especially from the SBSs. Thus, it is necessary to offload UEs to the less interference-prone mm-wave RAT to enhance the SINR in cities with dense roads. Clearly, increasing the mm-wave selection probability (with $G_0 = 30$ dBi) enhances the SINR (see Fig. 6a). However, in the following section we will see that, in presence of vehicular blockages and for sparse SBS deployments, the SINR in mm-wave band can be worse than the one perceived in the sub-6GHz band.

D. Slice-Aware RAT Selection

In this section, first, we discuss the effect of Q_R on the network performance, and accordingly, reveal the intuition behind the choice of the slice-aware RAT biasing.

Algorithm 1 Network-Side Pseudo-code

Obtain the data about expected vehicular density in the service area.
for each slice of QoS triplet $(\mathcal{B}, \mathcal{P}_C, \mathcal{P}_R) \in \mathcal{T}$ **do**
  Identify the set of biases $(0, Q_B)$ that satisfy $\mathcal{B}$, using (5).
  Identify the set of biases (Q_{C1}, Q_{C2}) that satisfy $\mathcal{P}_C$, using (12).
  Identify the set of biases (Q_{R1}, Q_{R2}) that satisfy $\mathcal{P}_R$, using (15).
  Obtain $Q_R^* \in (1, Q_B) \cap (Q_{C1}, Q_{C2}) \cap (Q_{R1}, Q_{R2})$ for maximizing $\mathcal{P}_C$ in (12) if URLLC/mMTC slice, or for maximizing $\mathcal{P}_R$ in (15) if eMBB slice, using random restart hill climbing.
  Broadcast Q_R^* within the slice.
end for

Algorithm 2 UE-Side Pseudo-code

Measure downlink sub-6GHz received powers, $P_{tv\mu}$, from all BSs.
if $P_{Mv\mu 1} \geq P_{Sv\mu 1}$ **then**
  Request to be associated to the strongest MBS.
else
  Request to be associated to the strongest SBS and measure the mm-wave power from it (P_{Svm1}).
  Obtain the RAT bias Q_R^* for the associated slice.
  if $P_{Sv\mu 1} \geq Q_R^* P_{Svm1}$ **then**
    Request to be served from SBS in sub-6GHz band.
  else
    Request to be served from SBS in mm-wave band.
  end if
end if

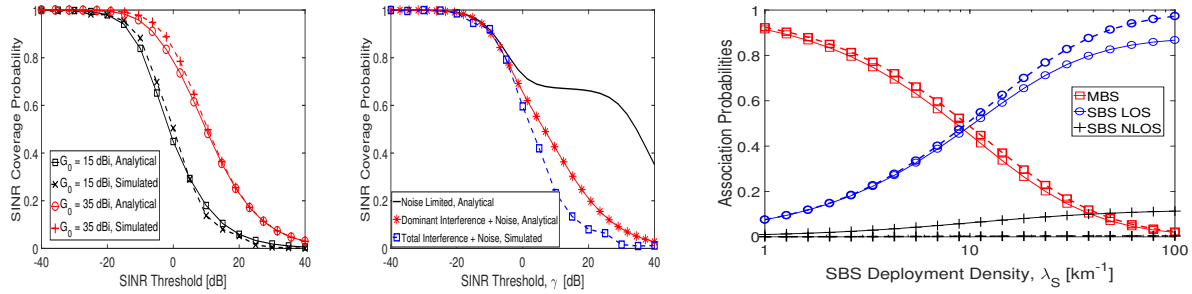

(a) (b) (c)

Fig. 4. (a) Validation of the model for the SINR coverage probability with $\lambda_S = 100$ km^{-1}, (b) Validation of the dominant interference model, $G_0 = 35$ dBi, $\lambda_S = 100$ km^{-1} and (c) Association probabilities of the UEs with varying SBS density (solid lines correspond to $\lambda_R = 15$ km^{-1}, dashed lines correspond to $\lambda_R = 5$ km^{-1}).

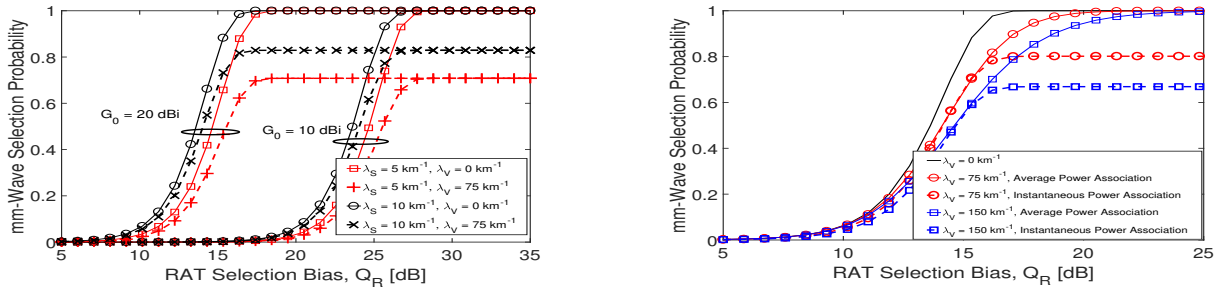

(a) (b)

Fig. 5. (a) Conditional mm-wave selection probability with RAT selection bias, (b) Comparison of different schemes of RAT selection, $G_0 = 20$ dBi and $\lambda_S = 10$ km^{-1}.

1) SINR Coverage: In Fig. 7, we plot the SINR coverage probability of the UEs at $\gamma = -10$ dB with varying Q_R for different vehicular blockage densities. We see that in the case where the roads are devoid of vehicles, the SINR coverage probability increases with Q_R for both dense (Fig. 7a) and sparse (Fig. 7b) deployment of SBSs, precisely due to the combined effects of LOS mm-wave signals and minimal interference in the mm-wave band.

As the λ_V increases (from 75 to 200 km^{-1}), aggressive mm-wave policy deteriorates the SINR coverage. As a result, for a given vehicular density in an urban area, there exists an optimal RAT selection bias that maximizes the SINR coverage. More interestingly, in Fig. 7b, we observe that in case of sparse deployments ($\lambda_S = 10$ km^{-1}), with very dense vehicular traffic ($\lambda_V = 200$ km^{-1}), higher biases decreases the system coverage. Thus, corresponding to a required threshold $\mathcal{P}_C^*$, the operator should select the RAT bias value from a range (Q_{C1}, Q_{C2}).

In Fig. 7c, we plot the vehicular blockage probability with varying Q_R. As Q_R increases, the blockage increases, due to the increased number of UEs served in the mm-wave band, which is prone to the vehicular blockage. Thus, UEs URLLC applications will necessarily need to operate below a bias threshold (say Q_B) governed by the current λ_V.

From Fig. 8a, we see that the rate coverage increases with Q_R even in the case of high λ_V (even though the SINR

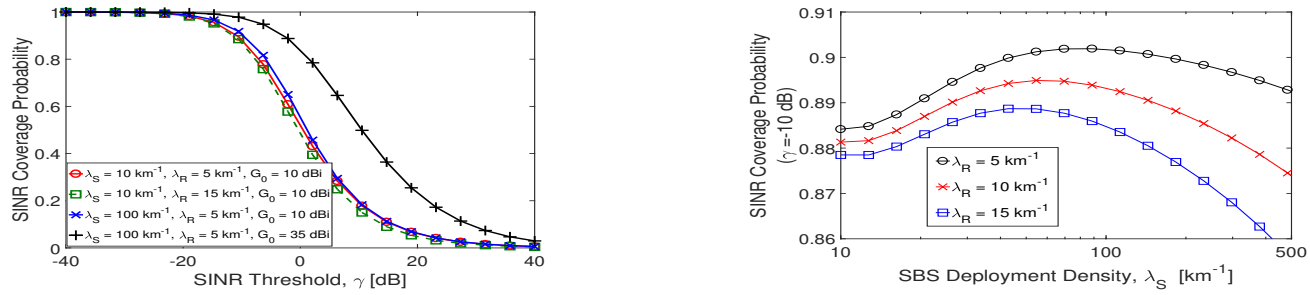

(a) (b)

Fig. 6. (a) SINR coverage probability of the UEs for different SBS deployment densities and road densities, (b) SINR coverage probability for the UEs at $\gamma = -10$ dB with respect to the SBS deployment density ($G_0 = 10$ dBi, $Q_R = 0$ dB).

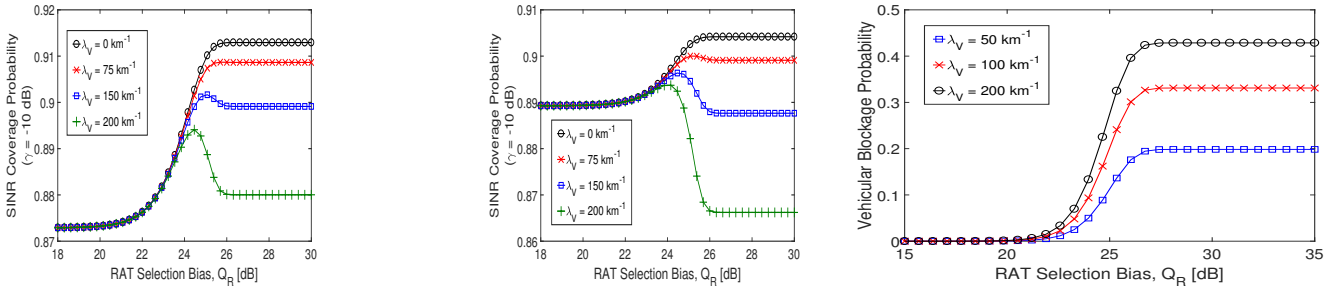

(a) (b) (c)

Fig. 7. SINR coverage probabilities for the UEs with varying RAT selection bias with $G_0 = 10$ dBi for different vehicular blockage densities, (a) $\lambda_S = 50$ km^{-1} and (b) $\lambda_S = 10$ km^{-1}. (c) Vehicular blockage probability with respect to RAT selection bias given that the UE is served with mm-wave RAT.

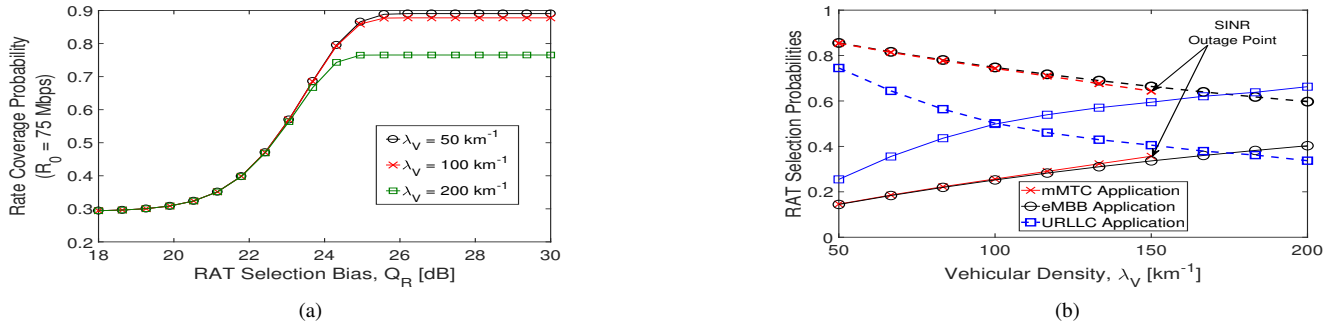

(a) (b)

Fig. 8. (a) Rate coverage probability for the UE for different vehicular blockage densities, $\lambda_S = 10$ km^{-1} and (b) Slice-aware RAT selection, solid lines denote the sub-6GHz association probabilities and the dotted lines denote the mm-wave association probabilities respectively.

coverage decreases, see Fig. 7a). This is due to the large bandwidth in the mm-wave band that compensates for the loss in SINR. However, operating at biases that result in very low SINR would result in service outage. As a result, it is necessary to optimize Q_R with respect to the data rate while satisfying the SINR constraints.

To give a better insight to the bias selection scheme, we illustrate our RAT selection protocol with three examples: 1) A slice for a URLLC service with $T^* = (0.001, 0.85, 0.5)$, 2) A slice for an mMTC service with $T^* = (0.1, 0.9, 0)$, and 3) A slice for an eMBB service with $T^* = (0, 0.85, 0.7)$. We assume a network with $\lambda_S = 10$ km^{-1}, $\lambda_R = 15$ km^{-1}, and $G_0 = 15$ dBi.

For example 1, $\mathcal{B}^*$ is 0.1%, which results in $Q_R^* = 19.7$ dB. This leads in a lower mm-wave selection probability (see Fig. 8b) as compared to the other applications. As the vehicular density increases, the maximum allowable Q_R to satisfy the vehicular blockage constraint gradually decreases, thereby further decreasing the mm-wave selection probability. For example 2, the $\mathcal{B}^*$ is less stringent (10%), whereas $\mathcal{P}_C^*$

is tighter (outage constraint equal to 10%). In case of low λ_V (e.g., 50 km^{-1}), the optimized bias is $Q_R^* = 25$ dB, which achieves an SINR coverage of more than 91%, with a mm-wave selection of over 80%. This is considerably higher than the URLLC applications. However, for $\lambda_V \geq 150$ km^{-1}, no feasible bias exists to satisfy the outage constraint, and the application cannot be supported with current network dimensioning. The vehicular density value after which the network is not able to sustain outage below 10% is shown in Fig. 8b. Finally, for example 3, the eMBB service does not have any vehicular blockage constraints. Thus, the bias for eMBB applications aims to maximize the rate coverage probability, while satisfying the outage constraint (here 15%). For $\lambda_V = 50$ km^{-1}, the optimized bias ($Q_R^* = 26.21$ dB) results in a slightly higher mm-wave selection probability than the mMTC application. As the vehicular traffic increases, the optimal bias value decreases (see Fig. 8b). However, as the outage constraint is not as stringent as the mMTC application of example 2, the UE can be served even under very high vehicular densities (e.g., $\lambda_V = 200$ km $^{-1}$).

E. System Design Insights

Finally, we outline the system design and dimensioning insights based on our results:

- In case the operator needs to prioritize mm-wave association for high-data rate services so as to free the sub-6GHz RAT for reliability specific applications, it needs to deploy more SBSs per road in a city with more roads. However, excessive deployment of SBSs degrades the SINR performance of the UEs. Thus, proper care must be taken of this tradeoff while dimensioning the cellular network.
- For aggressively offloading the UEs to mm-wave, increasing the directivity gain of the antenna is a more efficient mechanism than deploying more SBSs due to the deployment costs. However, in case of presence of vehicles, the mm-wave association saturates. This effect can be reduced by adopting an *averaged power RAT selection* instead of a more *instantaneous power RAT selection* at the cost of an increased access delay.
- Having a network-wide RAT selection bias will not be able to support a diverse plethora of applications. Hence, slice-aware RAT selection becomes necessary. For URLLC services, there exists a threshold of bias beyond which the blockage of the service becomes intolerable. For applications that require high SINR on the contrary, e.g., mMTC, there exist non-trivial biases that maximize the SINR.
- The bias values that maximize the downlink data rate may lead to excessive outage, and hence, we provided optimal bias values for rate coverage under outage constraints. If the operator wants to increase the rate coverage even further, e.g., for eMBB applications, it is important to develop efficient interference management mechanisms as increasing the deployment density simply degrades the SINR performance.

IX. Conclusion

In this paper, we have characterized a multi-tier network operating in multiple radio bands. We have provided realistic characterizations of the mm-wave interference and effect of vehicular blockage on the mm-wave RAT. First, from the perspective of the pedestrian UEs, we have analyzed the effect of the RAT selection bias on the mm-wave blockage, SINR coverage, and rate coverage probability under different vehicular densities. Accordingly, we have provided a slice-aware RAT selection strategy to jointly support URLLC, mMTC, and eMBB applications in future mm-wave sliced 5G networks. Finally, we have highlighted several key system design insights for an operator that aims to optimally serve a diverse variety of services. Our study provides a first investigation with respect to RAT multiplexing in the new radio. In future works, we plan to extend this analysis by considering additional QoS performance indicators such as latency and reliability.

Appendix A

Proof of Lemma 2: For the first part of the Lemma, let $\nu(x)$ be a positive measurable, radially symmetric function with bounded support. Let first assume the support to be a disk centered at origin with radius R. Now the function ν in our case is the SINR coverage probability (thus, $0 \leq \nu \leq 1$), and accordingly, the PGF is bounded below by 0 and decreases monotonically with R. The Lemma thus follows from the monotone convergence theorem with $R \to \infty$. We have:

$$G_{\phi_S}(\nu) = \mathbb{E}\left[\prod_{x\in\phi_S} \nu(x)\right] = \int \prod_{x\in\phi_S} \nu(x)\phi_S(dx),$$
$$\stackrel{a}{=} \sum_{n=0}^{\infty} \frac{\exp\left(-2\pi R\lambda_R\right)}{n!\, R^n} \left(2\pi R\lambda_R\right)^n$$
$$\int_{r_1,r_2,\ldots,r_n=0}^{R} \left(\prod_{i=1}^{n} \int_{\mathbb{R}} \prod_{x\in\phi_i} \nu(x)\phi_i(dx)\right) dr_1,\ldots,dr_n.$$

where (a) is obtained by conditioning on the number of roads (n) and on the distances of the roads ($r_1,\ldots,r_n$)[8]. The number of lines crossing a circle with radius R is Poisson distributed with parameter $2\pi R\lambda_R$. Now, for each of the lines, we calculate the PGF as [22]:

$$\int \prod_{x\in\phi_i} \nu(x)\phi_i(dx) =$$
$$\exp\left(-2\lambda_S \int_0^{\sqrt{R^2-r^2}} 1-\nu\left(\sqrt{r_i^2+t^2}\right) dt\right).$$

As a result, we have:

$$G_{\phi_S}(\nu) = \sum_{n=0}^{\infty} \frac{\exp(-2\pi R\lambda_R)\left(2\pi\lambda_R\right)^n}{n!}$$
$$\left(\int_0^R \exp\left(-2\lambda_S \int_0^{\sqrt{R^2-r^2}} 1-\nu\left(\sqrt{r^2+t^2}\right) dt\right) dr\right)^n.$$

Using the series expansion of $\exp(\cdot)$, completes the proof. For the second part of the lemma, without loss of generality, assume that the line passes through $(d,0)$. A point on the line at a distance t from $(d,0)$ is at a distance $r = \sqrt{(d+t\cos\theta)^2 + (t\sin\theta)^2}$ from the origin, where θ is the orientation of the line. Taking the PGF along all such points completes the proof.

[8]By convention, we assume the value inside the inner integral to be 1 when $n = 0$.

APPENDIX B

Proof of Lemma 3: Assume that the nearest NLOS SBS is at a distance x from the typical UE. Then, the ball $\mathcal{B}(o,x)$ does not contain any NLOS SBS. A randomly orientated line at a distance r from the origin, has a chord length of $2\sqrt{x^2-r^2}$, and a void probability $\exp(-2\lambda_S\sqrt{x^2-r^2})$. As a result, the probability of no points falling in this ball, averaged over the number of lines, is:

$$F_{d_{SN1}}(x) = \sum_{n=0}^{\infty} \frac{(2\pi\lambda_R x)^n \exp(-2\pi\lambda_R x)}{n!\,(x^n)} \left[\int_{r_1,r_2,\ldots,r_n=0}^{x} \prod_{i=1}^{n} \exp\left(-2\lambda_S\sqrt{x^2-r_i^2}\right) dr_i\right]$$
$$= \sum_{n=0}^{\infty} \frac{(2\pi\lambda_R x)^n \exp(-2\pi\lambda_R x)}{n!\,(x^n)} \left[\int_0^x \exp\left(-2\lambda_S\sqrt{x^2-r^2}\right) dr\right]^n. \quad (17)$$

This is the CDF of the distance. The PDF is then obtained by differentiating with respect to x.

For the remaining distributions, i.e., for $\{t,v\} \neq \{SN\}$, the expressions for $f_{d_{tv1}}$, can be obtained by differentiating the void probabilities of the corresponding processes [22].

APPENDIX C

Proof of Proposition 1: In Fig. 2, the UE at O at a distance d from its serving SBS AB is in NLOS if a vehicle exists in between the UE and AB within a distance d_0. From the similarity of triangles ABO and $A'B'O$, it follows that $d_0 = \frac{h_V}{h_B}d$. The link between O and AB is in LOS if none of the roads crossing $B'O$ is occupied by a vehicle. Now, the number of roads n passing through the region d_0 is Poisson distributed with intensity $\lambda_R d_0$. Since the fraction of the roads occupied by the vehicles is $\lambda_V' = L_V\lambda_V$, the probability of blockage due to one road is $1-\lambda_V'$. We have: $\mathcal{L}(d) = \mathbb{E}_n[(1-\lambda_V')^n] = \sum_{n=0}^{\infty}(1-\lambda_V')^n \frac{(\lambda_R d_0)^n \exp(-\lambda_R d_0)}{n!} = \exp\left(-\lambda_V'\lambda_R\frac{h_V}{h_B}d\right)$. $\mathcal{B}(Q_R)$ is then calculated as:

$$\mathcal{B}(Q_R) = \mathbb{E}_{d_{SL1}}\left[(1-\mathcal{L}(d_{SL1}))|\mathbb{1}_m(d_{SL1},Q_R)\right] = \int_0^H \left(1-\exp\left(-\lambda_R\lambda_V'\frac{h_V}{h_B}x\right)\right) f_{d_{SL1}}(x)dx,$$

where $\mathbb{1}_m$ represents the indicator function for mm-wave operation.

APPENDIX D

Proof of Lemma 5: From the typical SBS, let the distance to its n-th neighbor be given by d_n (see Fig. 3a for notations). Thus, the distance of the typical SBS from the center of $(n-1)$-th and n-th neighboring SBS is given by $\bar{d}_n = \frac{d_n+d_{n-1}}{2}$. Let the depression angle from the top of the typical SBS to a UE located at its boundary be ϕ. Clearly, $\phi = \arctan\left(\frac{d_a}{2h_B}\right) - \frac{\theta}{2}$. Let the distance of the point where the serving beam reaches the ground from the typical SBS be denoted by $x = h_B\tan(\phi+\theta)$. Thus, the probability of the typical SBS causing interference in the n-th neighbor is given by:

$$\mathbb{P}(x \geq \bar{d}_n) = \mathbb{P}\left(h\tan\left(\arctan\left(\frac{d_a}{2h_B}\right)+\frac{\theta}{2}\right) \geq \frac{d_n+d_{n-1}}{2}\right),$$
$$= \mathbb{P}\left(d_a \geq 2h_B\left[\tan\left(\arctan\left(\frac{d_n+d_{n-1}}{2h}\right)-\frac{\theta}{2}\right)\right]\right).$$

Using the void probability and the expectation with respect to the joint distribution of d_n and d_{n-1} completes the proof. The latter is derived as follows (assuming $d_n = Y$ and $d_{n-1} = X$): $f_{Y|X}(y|x)f_X(x) = \frac{d}{dy}\left[\exp\left(\lambda_S(y-x)\right)\right]\frac{\exp(-\lambda_S x)(\lambda_S x)^{n-2}}{(n-2)!} = \frac{\lambda_S^2\exp(-\lambda_S y)}{(n-2)!}(\lambda_S x)^{n-2}$.

APPENDIX E

Proof of Lemma 6: Let the typical UE U_1 be located at a distance d_1 from its serving BS B_1 (the BS on the right in Fig. 3b). We are interested in the probability that U_1 experiences interference from the neighboring SBS B_2 serving a UE U_2. We define *spillover* as the region of interference that an SBS creates in a neighboring cell while serving a UE. Now, B_2 causes spillover to the coverage area of B_1 if the extremest point of its beam crosses the cell boundary, i.e., if the position of U_2 from B_2 is greater than some value (say d'). The maximum distance of U_2 from B_2 is $\frac{d_a}{2}$. Thus, there is spillover, if the UE U_2 lies in the region $d' \leq d_2 \leq \frac{d_a}{2}$. The probability that at least one such UE exists is obtained using the void probability of the UE PPP and is given by $\left(1-\exp\left(\lambda_U\left(\frac{d_a}{2}-d'\right)\right)\right)$. The extent of spillover (s) to the coverage area of B_1, from B_2 serving U_2 is:

$$s = GC - \frac{d_a}{2} = h\tan\left(\frac{\theta}{2}+\phi\right) - \frac{d_a}{2} = h\tan\left(\frac{\theta}{2}+\arctan\left(\frac{d_2}{h}\right)\right) - \frac{d_a}{2}, \quad (18)$$

where ϕ is the angle of depression from the top of B_2 to U_2 on the ground. Now, d' is then obtained from the condition $s=0$, i.e., the location of U_2, beyond which the coverage area of B_1 experiences spillover from B_2. This results in: $d' = h\tan\left(\arctan\frac{d_a}{2h} - \frac{\theta}{2}\right)$. To keep our analysis tractable, we assume that B_2 does not create a spillover in the coverage region of B_1, when serving the UEs on its left. For practical values, this conditions always holds. For example, with $h_B =$ 10 m, and θ of 10 degrees, we have $d_a \geq 1.75$ m. For the SBS densities considered throughout this paper ($\lambda_S < 100$ km^{-1}), this holds with a high probability (≥ 0.85). Thus we have: $d' \geq 0 \implies d_a \geq 2h\tan\left(\frac{\theta}{2}\right)$. The probability that U_1 is located in the spillover region, given that the spillover is s, is:

$$\mathbb{P}(U_1 \in s) = \begin{cases} \mathbb{P}\left(d_1 \geq \frac{d_a}{2}-s\right) = \\ \exp\left(-\lambda_S\left(\frac{d_a}{2}-s\right)\right); & s \leq \frac{d_a}{2} \\ 1; & s \geq \frac{d_a}{2} \end{cases},$$

Now we substitute s from (18) in (19), and take the expectation with respect to d_a and d_2: $f_{d_a,d_2}(x,y) = \lambda_U\lambda_S\exp\left(-\lambda_U\left(\frac{x}{2}-y\right)\right)\exp(-\lambda_S x), \quad y \leq \frac{x}{2}$.

APPENDIX F

Proof of Proposition 2: The UE association probabilities with a LOS and NLOS MBS and LOS SBS are:

$$\begin{aligned}\mathcal{P}_{ML} &= \mathcal{T}\mathbb{P}(P_{ML1} \geq P_{SL1}, P_{ML1} \geq P_{SN1}),\\ \mathcal{P}_{MN} &= (1-\mathcal{T})\,\mathbb{P}(P_{MN1} \geq P_{SL1}, P_{MN1} \geq P_{SN1}),\\ \mathcal{P}_{SL} &= \mathcal{T}\mathbb{P}(P_{SL1} \geq P_{ML1}, P_{SL1} \geq P_{SN1}) +\\ &\quad (1-\mathcal{T})\,\mathbb{P}(P_{SL1} \geq P_{MN1}, P_{SL1} \geq P_{SN1}),\end{aligned}$$

where $\mathcal{T} = \mathbb{E}[\mathbb{1}(ML)]$ is the probability of the existence of at least one LOS MBS. In our model, a signal from a LOS MBS will be received with higher power than one from any NLOS MBS. In the following, we show how to calculate $\mathbb{P}_{ML}$. The other probabilities follow similarly.

$$\begin{aligned}&\mathcal{P}_{ML} = \mathbb{E}\left[\mathbb{1}(ML)\right]\mathbb{P}\left(P_{ML1} > P_{SL1}, P_{ML1} > P_{SN1}\right)\\ &= \mathbb{E}\left[\mathbb{1}(ML)\right]\left(\mathbb{P}(P_{ML1} > P_{SL1}, P_{SL1} > P_{SN1}) + \right.\\ &\left.\mathbb{P}(P_{ML1} > P_{SN1}, P_{SN1} > P_{SL1})\right)\\ &= \mathbb{E}\left[\mathbb{1}(ML)\right]\left(\mathbb{P}\left(K_\mu P_M d_{ML1}^{-\alpha_{ML\mu}} > K_\mu P_S d_{SL1}^{-\alpha_{SL\mu}},\right.\right.\\ &\left.K_\mu P_S d_{SL1}^{-\alpha_{SL\mu}} > K_\mu P_S d_{SN1}^{-\alpha_{SN\mu}}\right) + \mathbb{P}\left(K_\mu P_M d_{ML1}^{-\alpha_{ML\mu}} > \right.\\ &\left.\left.K_\mu P_S d_{SN1}^{-\alpha_{SN\mu}}, K_\mu P_S d_{SN1}^{-\alpha_{SN\mu}} > K_\mu P_S d_{SL1}^{-\alpha_{SL\mu}}\right)\right)\\ &= \mathbb{E}\left[\mathbb{1}(ML)\right]\left(\mathbb{E}_{d_{ML1},d_{SN1}}\left[\exp\left(-2\lambda_S\left(d_{SN1}^{\frac{\alpha_{SN\mu}}{\alpha_{SL\mu}}} - \right.\right.\right.\right.\\ &\left.\left.\left.\left.\left(\frac{P_S}{P_M} d_{ML1}^{\alpha_{ML\mu}}\right)^{\frac{1}{\alpha_{SL\mu}}}\right)\right)\mathcal{T}_1(d_{ML1})\right] +\\ &\mathbb{E}_{d_{ML1},d_{SL1}}\left[\left(F_{d_{SN1}}\left(d_{SL1}^{\frac{\alpha_{SL\mu}}{\alpha_{SN\mu}}}\right) - \right.\right.\\ &\left.\left.F_{d_{SN1}}\left(\left(\frac{P_S}{P_M} d_{ML1}^{\alpha_{ML\mu}}\right)^{\frac{1}{\alpha_{SN\mu}}}\right) F_{d_{SN1}}\left(x^{\frac{\alpha_{SL\mu}}{\alpha_{SN\mu}}}\right)\right)\right]\Bigg).\end{aligned}$$

APPENDIX G

Proof of Proposition 3: The probability of mm-wave association based on instantaneous power RAT selection is:

$$\begin{aligned}\mathcal{P}_m &= \mathbb{E}\left[\mathcal{L}(d_{SL1})\right]\mathbb{P}(r = mm | t = SL) =\\ &\mathbb{E}\left[\mathcal{L}(d_{SL1})\right]\mathbb{P}\left(d_{SL1} < \left(\frac{K_m G_0 Q_R}{K_\mu}\right)^{\frac{1}{\alpha_{SLm}-\alpha_{SL\mu}}}\right)\\ &= \frac{2h_B\lambda_S}{\lambda'_V h_V \lambda_R + 2h_B\lambda_S}\\ &\left[1 - \exp\left(-2\lambda_S\left(\frac{K_m G_0 Q_R}{K_\mu}\right)^{\frac{1}{\alpha_{SLm}-\alpha_{SL\mu}}}\right)\right], \quad (19)\end{aligned}$$

where $\mathbb{E}\left[\mathcal{L}(d_{SL1})\right]$ refers to the average probability that the UE experiences a LOS path from the strongest SBS, which is calculated by taking the expectation of $\mathcal{L}(d_{SL1})$ (see Proposition 1) with respect to the distance d_{SL1}, i.e., $\mathbb{E}\left[\mathcal{L}(d_{SL1})\right] = \mathbb{E}_{d_{SL1}}\left[\exp\left(-\lambda'_V\lambda_R\frac{h_V}{h_B}d_{SL1}\right)\right] = \frac{2h_B\lambda_S}{\lambda'_V h_V\lambda_R + 2h_B\lambda_S}$. In case of association based on averaged power RAT selection, we have:

$$\begin{aligned}\bar{\mathcal{P}}_m &= \mathbb{P}(Q_R K_m G_0 P_S d_{SL1}^{-\alpha_{SLm}} \mathbb{P}_L(d_{SL1}) > K_\mu P_S d_{SL1}^{-\alpha_{SL\mu}},\\ &= \mathbb{P}\left(d_{SL1} \leq \frac{h_B\left(\alpha_{SLm} - \alpha_{SL\mu}\right)}{\lambda'_V\lambda_S h_V}\right.\\ &\left.\mathcal{W}\left(\frac{\lambda'_V\lambda_S h_v}{h_B(\alpha_{SLm}-\alpha_{SL\mu})}\left(\frac{K_\mu}{K_m G_0 Q_R}\right)^{\frac{1}{\alpha_{SL\mu}-\alpha_{SLm}}}\right)\right).\end{aligned}$$

APPENDIX H

Proof of Theorem 1: A UE located at d_{SL1} from its serving SBS experiences mm-wave interference from an SBS located at d_{SL2} from it, when 1) the UE lies in the spillover region of the interfering SBS and 2) the interfering link is not blocked by moving vehicles. Accordingly:

$$\begin{aligned}SINR_{SLm} =& \frac{P_S G_0 K_m h_{mSL1} d_{SL1}^{-\alpha_{SLm}}}{\sigma_{mm}^2 + P_S G_0 K_m h_{mSL2} d_{SL2}^{-\alpha_{SLm}}}\\ & p_G(d_{SL1}, d_{SL2})\mathcal{L}(d_{SL1})\mathcal{L}(d_{SL2}) +\\ & \frac{P_S G_0 K_m h_{SL1} d_{SL1}^{-\alpha_{SLm}}}{\sigma_{mm}^2}\mathcal{L}(d_{SL1})\\ & \left(1 - p_G(d_{SL1}, d_{SL2})\mathcal{L}(d_{SL2})\right),\end{aligned}$$

where $\mathcal{L}(d_{SL1})$ and $\mathcal{L}(d_{SL2})$ are given by Proposition 1, and $p_G(d_{SL1}, d_{SL2})$ is the probability that the typical UE experiences mm-wave interference. Although p_G depends on d_{SL1} and d_{SL2}, the SINR coverage probability can be approximated by using the expression of $\bar{p}_G$ from (7) as:

$$\begin{aligned}&\mathbb{P}\left(SINR_{SLm} \geq \gamma\right) \overset{(a)}{\geq}\\ &\mathbb{P}\left(\frac{P_S G_0 K_m h_{mSL1} d_{SL1}^{-\alpha_{SLm}}\mathcal{L}(d_{SL1})}{\sigma_{mm}^2 + P_S G_0 K_m h_{mSL2} d_{SL2}^{-\alpha_{SLm}} p_G(d_{SL1}, d_{SL2})\mathcal{L}(d_{SL2})}\right.\\ &\left.\geq \gamma\right)\\ &\overset{(b)}{\geq}\mathbb{P}\left(\frac{P_S G_0 K_m h_{mSL1} d_{SL1}^{-\alpha_{SLm}}\mathcal{L}(d_{SL1})}{\sigma_{mm}^2 + P_S G_0 K_m h_{mSL2} d_{SL2}^{-\alpha_{SLm}}\bar{p}_G\mathcal{L}(d_{SL2})} \geq \gamma\right)\\ &=\mathbb{P}\left(h_{mSL1} \geq \right.\\ &\left.\frac{\gamma\left(\sigma_{mm}^2 + P_S G_0 K_m h_{mSL2} d_{SL2}^{-\alpha_{SLm}}\bar{p}_G\mathcal{L}(d_{SL2})\right)}{P_S G_0 K_m d_{SL1}^{-\alpha_{SLm}}\mathcal{L}(d_{SL1})}\right),\end{aligned}$$

The steps (a) and (b) follow from Jensen's inequality and the final expression follows by taking the PGF with respect to the channel power h_{mSL1}. Subsequently, taking the expectation with respect to the joint distribution of $d_{SL1} = X$ and $d_{SL2} = Y$, we complete the proof:

$$\begin{aligned}f_{X,Y}(x,y) &= f_{Y|X}(y|x)f_X(x)\\ &= \frac{-\partial}{\partial y}\mathbb{P}\left(Y < y | X = x\right)\frac{-\partial}{\partial x}\mathbb{P}\left(X < x\right)\\ &= \frac{-\partial}{\partial y}\left[\exp\left(-\lambda_S(x+y-2x)\right)\right]\frac{-\partial}{\partial x}\left[\exp\left(-2\lambda_S x\right)\right]\\ &= 2\lambda_S^2\exp(-\lambda_S(x+y)).\end{aligned}$$

The sub-6GHz association cases follow on similar lines as given in [6].

REFERENCES

[1] G. Ghatak and A. De Domenico and M. Coupechoux, "Modeling and Analysis of HetNets with mm-Wave Multi-RAT Small Cells Deployed along Roads," *IEEE Globecom*, pp. 1–7, Dec. 2017.

[2] J. G. Andrews, *et al.*, "What Will 5G Be?" *IEEE J. Sel. Areas Commun.*, vol. 32, no. 6, pp. 1065–1082, June 2014.

[3] A. Ghosh, *et al.*, "Millimeter-Wave Enhanced Local Area Systems: A High-Data-Rate Approach for Future Wireless Networks," *IEEE J. Sel. Areas Commun.*, vol. 32, no. 6, pp. 1152–1163, June 2014.

[4] T. S. Rappaport, *et al.*, "Millimeter Wave Mobile Communications for 5G Cellular: It Will Work!" *IEEE Access*, vol. 1, pp. 335–349, 2013.

[5] Y. Li, *et al.*, "On the Initial Access Design in Millimeter Wave Cellular Networks," in *IEEE Globecom Wkshps.*, Dec. 2016, pp. 1–6.

[6] G. Ghatak, A. De Domenico, and M. Coupechoux, "Coverage Analysis and Load Balancing in HetNets with mmWave Multi-RAT Small Cells," *IEEE Trans. Wireless Commun.*, vol. 17, no. 5, pp. 3154–3169, May 2018.

[7] P. Demestichas, *et al.*, "5G on the Horizon: Key Challenges for the Radio-Access Network," *IEEE Veh. Technol. Mag.*, vol. 8, no. 3, pp. 47–53, Sep. 2013.

[8] X. Foukas, *et al.*, "Network Slicing in 5G: Survey and Challenges," *IEEE Commun. Mag.*, vol. 55, May 2017.

[9] 3GPP TSG SA, "TS 23.501, System Architecture for the 5G system; Stage 2, (Release 16)," Apr. 2019.

[10] J. G. Andrews, F. Baccelli, and R. K. Ganti, "A Tractable Approach to Coverage and Rate in Cellular Networks," *IEEE Trans. Commun.*, vol. 59, no. 11, pp. 3122–3134, Nov. 2011.

[11] T. Bai and R. W. Heath, "Coverage and Rate Analysis for Millimeter-Wave Cellular Networks," *IEEE Trans. Wireless Commun.,*, vol. 14, no. 2, pp. 1100–1114, Feb. 2015.

[12] M. Di Renzo, "Stochastic Geometry Modeling and Analysis of Multi-Tier Millimeter Wave Cellular Networks," *IEEE Trans. Wireless Commun.*, vol. 14, no. 9, pp. 5038–5057, Sep. 2015.

[13] H. Elshaer, *et al.*, "Downlink and Uplink Cell Association With Traditional Macrocells and Millimeter Wave Small Cells," *IEEE Trans. Wireless Commun.*, vol. 15, no. 9, pp. 6244–6258, Sept. 2016.

[14] Y. J. Chun, M. O. Hasna, and A. Ghrayeb, "Modeling heterogeneous cellular networks interference using poisson cluster processes," *IEEE J. Sel. Areas Commun.*, vol. 33, no. 10, pp. 2182–2195, 2015.

[15] C. Gloaguen, *et al.*, "Analysis of shortest paths and subscriber line lengths in telecommunication access networks," *Networks and Spatial Economics*, vol. 10, no. 1, pp. 15–47, 2010.

[16] F. Morlot, "A population model based on a Poisson line tessellation," in *IEEE WiOpt*, May 2012, pp. 337–342.

[17] C.-S. Choi and F. Baccelli, "An Analytical Framework for Coverage in Cellular Networks Leveraging Vehicles," *IEEE Trans. Commun.*, vol. 66, no. 10, pp. 4950–4964, Oct. 2018.

[18] A. Tassi, *et al.*, "Modeling and design of millimeter-wave networks for highway vehicular communication," *IEEE Trans. Veh. Technol.*, vol. 66, no. 12, pp. 10 676–10 691, Dec. 2017.

[19] Qualcomm, "Mobilizing 5G NR Millimeter Wave: Network Coverage Simulation Studies for Global Cities," Oct. 2017. [Online]. Available: https://www.qualcomm.com/media/documents/files/white-paper-5g-nr-millimeter-wave-network-coverage-simulation.pdf

[20] H. Shokri-Ghadikolaei, L. Gkatzikis, and C. Fischione, "Beam-searching and transmission scheduling in millimeter wave communications," in *IEEE ICC, 2015*, pp. 1292–1297.

[21] 3GPP TSG RAN, "TR 38.913, Study on Scenarios and Requirements for Next Generation Access Technologies ," *v15*, June 2018.

[22] S. N. Chiu, *et al.*, *Stochastic geometry and its applications*. John Wiley & Sons, 2013.

[23] J. G. Andrews, *et al.*, "Modeling and analyzing millimeter wave cellular systems," *IEEE Trans. Commun.*, vol. 65, no. 1, pp. 403–430, Jan. 2017.

[24] 3GPP TSG RAN, "TR 36.814, E-UTRA; Further advancements for E-UTRA physical layer aspects," *v9.0.0*, Mar. 2010.

[25] White Paper, "5G Channel Model for bands up to 100 GHz," *http://www.5gworkshops.com/5gcm.html*.

[26] 3GPP TSG RAN, "TR 36.873, Study on 3D Channel Model for LTE (Release 12)," *v9.0.0*, Sept. 2014.

[27] T. Bai, R. Vaze, and R. W. Heath, "Analysis of Blockage Effects on Urban Cellular Networks," *IEEE Trans. Wireless Commun.*, vol. 13, no. 9, pp. 5070–5083, Sep. 2014.

[28] J. Harri, F. Filali, and C. Bonnet, "Mobility models for vehicular ad hoc networks: a survey and taxonomy," *IEEE Commun. Surveys Tuts.*, vol. 11, no. 4, Fourth 2009.

[29] M. K. Samimi and T. S. Rappaport, "3-D Millimeter-Wave Statistical Channel Model for 5G Wireless System Design," *IEEE Trans. Microw. Theory Tech.*, vol. 64, no. 7, pp. 2207–2225, July 2016.

[30] H. Zhao, *et al.*, "28 GHz millimeter wave cellular communication measurements for reflection and penetration loss in and around buildings in New York City," in *IEEE ICC*, June 2013, pp. 5163–5167.

[31] P. Popovski, *et al.*, "Wireless access for ultra-reliable low-latency communication: Principles and building blocks," *IEEE Netw.*, vol. 32, no. 2, pp. 16–23, Mar. 2018.

[32] EU-Commission *et al.*, "Regulation (eec) no 4064/89 merger procedure," *Case No COMP/JV*, 2000.

[33] C.-P. Li, *et al.*, "5g ultra-reliable and low-latency systems design," in *EuCNC*, June 2017, pp. 1–5.

[34] 3GPP TSG RAN, "TR 38.900, Study on channel model for frequency spectrum above 6 GHz," *v14.1.0*, September 2016.

Dr. Gourab Ghatak received his M.Tech degree from IIT Kanpur in 2015 and his PhD degree from CEA, Leti, France and from Université Paris Saclay, France in 2019. He is currently an Assistant Professor at the department of ECE in Indraprastha institute of information technology Delhi (IIIT-D), India. His research interests include stochastic geometry, millimeter-wave communications, 5G network planning, and signal processing for 5G waveforms.

Dr. Antonio De Domenico received his M.Sc. and Ph.D. degrees in telecommunication engineering in 2008 and 2012 from the University of Rome "La Sapienza" and the University of Grenoble, respectively. Since 2009, he has worked with the CEA-LETI – MINATEC, Grenoble, France, as a research engineer. His research topics are cloud enabled heterogeneous wireless networks, millimeter-wave-based communications, machine learning, and green communications. He is the main inventor or co-inventor of twelve patents. In 2017, Antonio has been awarded by the CEA Enhanced Eurotalents Programme. In 2018, he was a visiting researcher in the Communications Group of the Department of Electrical and Computer Engineering at the University of Toronto.

Prof. Marceau Coupechoux is Professor at Telecom ParisTech and Professeur Chargé de Cours at Ecole Polytechnique. He obtained his Master from Telecom ParisTech (1999) and from University of Stuttgart (2000), his Ph.D. from Institut Eurecom (2004), his Habilitation from University Pierre et Marie Curie (2015). From 2000 to 2005, he was with Alcatel-Lucent (in Bell Labs former Research & Innovation and then in the Network Design department). He was Visiting Scientist at the Indian Institute of Science, Bangalore, India, in 2011-2012. He has been General Co-Chair of WiOpt 2017 and Gamenets 2019. In the Computer and Network Science department of Telecom ParisTech, he is working on cellular networks, wireless networks, ad hoc networks, cognitive networks, internet of things, focusing mainly on performance evaluation, optimization and resource management.